HAL open science

Dynamics of epidemic spreading on connected graphs

Christophe Besse, Grégory Faye

▶ To cite this version:

Christophe Besse, Grégory Faye. Dynamics of epidemic spreading on connected graphs. Journal of Mathematical Biology, 2021, 82 (6), pp.52. 10.1007/s00285-021-01602-5 . hal-03019230

HAL Id: hal-03019230

https://hal.science/hal-03019230v1

Submitted on 23 Nov 2020

HAL is a multi-disciplinary open access archive for the deposit and dissemination of scientific research documents, whether they are published or not. The documents may come from teaching and research institutions in France or abroad, or from public or private research centers.

L'archive ouverte pluridisciplinaire **HAL**, est destinée au dépôt et à la diffusion de documents scientifiques de niveau recherche, publiés ou non, émanant des établissements d'enseignement et de recherche français ou étrangers, des laboratoires publics ou privés.

Dynamics of epidemic spreading on connected graphs

Christophe Besse & Grégory Faye[1]

[1]CNRS, UMR 5219, Institut de Mathématiques de Toulouse, 31062 Toulouse Cedex, France

November 23, 2020

Abstract

We propose a new model that describes the dynamics of epidemic spreading on connected graphs. Our model consists in a PDE-ODE system where at each vertex of the graph we have a standard SIR model and connexions between vertices are given by heat equations on the edges supplemented with Robin like boundary conditions at the vertices modeling exchanges between incident edges and the associated vertex. We describe the main properties of the system, and also derive the final total population of infected individuals. We present a semi-implicit in time numerical scheme based on finite differences in space which preserves the main properties of the continuous model such as the uniqueness and positivity of solutions and the conservation of the total population. We also illustrate our results with a selection of numerical simulations for a selection of connected graphs.

AMS classification: 34D05, 35Q92, 35B40, 92-10, 92D30.

Keywords: SIR model, graph, diffusion equation.

1 Introduction

Classical SIR compartment models are cornerstone models of epidemiology which allow one to study the evolution of an infected population at a given spatial scale (e.g. whole countries, regions, counties or cities). Such models date back to the pioneer work of Kermack and McKendrick [15] and describe the evolution of susceptible (S) and infected (I) populations which eventually become removed (R) via systems of ordinary differential equations which typically take the form

$$\begin{cases} S'(t) = -\tau S(t)I(t), \\ I'(t) = \tau S(t)I(t) - \eta I(t), \\ R'(t) = \eta I(t), \end{cases} \tag{1.1}$$

where $\tau > 0$ is a contact rate between susceptible and infected populations, and $1/\eta > 0$ is the average infectious period; see [12] for a review on SIR models. These models have been used in the

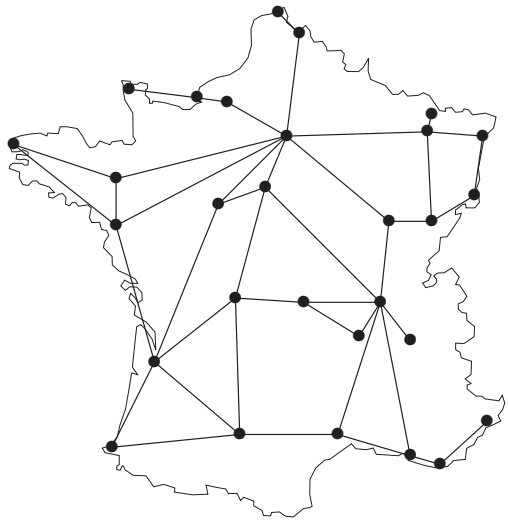

Figure 1: *Map of France with an illustration of a connected graph connecting major cities.*

past to reproduce data of epidemic outbreaks such as the bubonic plague [15], malaria [19], SARS influenza [6, 18] and most recently COVID-19 [16, 20, 21]; see also [20] for other applications.

In classical SIR models such as (1.1), interactions among the infected population are oversimplified, and when taken into account they typically involve transfer matrices of populations of infected between various uniform patches [17, 18, 26]. Our interest lies in the understanding of the intricate interplay between spatial effects and heterogeneous interactions among infected populations. Schematically, we propose a model composed of cities linked by a given transportation network (roads, railroads or rivers), see Figure 1 for an illustration in the case of France. It will turn out that the appropriate theoretical framework will be graph theory where each vertices of the graph will be thought as the cities and the edges the lines of transportation. In a first approximation, we will assume that infected populations are only subject to spatial diffusion along the lines, as it is traditionally assumed in classical spatial SIR models [1, 3, 9, 22]. As a consequence, in our model, the dynamics of the epidemic only takes place in the cities. Interactions are then modeled by flux exchanges between cities and lines where we assume that some fraction of infected individuals can either leave a city to be on a line, or leave a line and stop in a city, or pass from one line to another through a city. The typical question that we address here can easily be stated as follows. Given a connected graph of cities linked by roads and an initial configuration of infected individuals, how does the epidemic spread into the network and what is the eventual final configuration of the infected population? Our aim here is to gain insight into this spreading aspect at the fundamental mathematical level of a SIR type model that incorporates the possibility of infected individuals to travel along a specific given transportation network.

Our framework is at the crossroad of models that take into account lines of transportation such as recent reaction-diffusion models that study propagation of epidemics along lines with fast diffusion [3] and models that incorporate networks with more sophisticated interactions dynamics [2, 4, 5, 25]. On a formal level, our proposed model can be thought of as being a one-dimensional version of

the planar reaction-diffusion system of [3] with a line of fast diffusion in the case of one city and one line of transportation. Actually, the graph structure of the transportation network provides a natural embedding into a planar spatial domain. From a mathematical point of view, our model shares also some similarities with the PDE-ODE model of [8] which studies the spread of airborne diseases where the movement of pathogens in the air is assumed to follow a linear diffusion.

2 Model formulation and main results

Throughout, we denote by $\mathcal{G} = (\mathcal{V}, \mathcal{E})$ a compact metric graph, *i.e.* a collection of vertices $\mathcal{V}$ and edges $\mathcal{E}$ and further assume that $\mathcal{G}$ is finite and connected. Each edge $e \in \mathcal{E}$ is identified with a segment $\Omega_e = [0, \ell_e]$ with $\ell_e \in (0, \infty)$, where ℓ_e is the finite length of the edge. A real valued function $u : \mathcal{G} \longrightarrow \mathbb{R}$ is a collection of one dimensional maps defined for each edge $e \in \mathcal{E}$:

$$u_e : \Omega_e \longrightarrow \mathbb{R}.$$

For future references, we define $BC(\mathcal{G}, \mathbb{R})$ the space of bounded continuous functions on $\mathcal{G}$ as

$$BC(\mathcal{G}, \mathbb{R}) := \bigoplus_{e \in \mathcal{E}} BC(\Omega_e, \mathbb{R}),$$

and similarly $BC^k(\mathcal{G}, \mathbb{R})$ with $k \geq 1$. We define the L^∞ norm on $\mathcal{G}$ for $u \in BC(\mathcal{G}, \mathbb{R})$ as

$$\|u\|_\infty := \max_{e \in \mathcal{E}} \sup_{x \in \Omega_e} |u_e(x)|.$$

2.1 A SIR model on compact connected graph

Given a graph $\mathcal{G}$, we let $X_v(t) := (S_v(t), I_v(t), R_v(t)) \in \mathbb{R}^3$, for each $v \in \mathcal{V}$, where $S_v(t)$ represents the population of susceptible individuals, $I_v(t)$ the population of infected individuals and $R_v(t)$ the population of susceptible individuals at vertex $v \in \mathcal{V}$ and time $t > 0$. We assume that X_v evolves according to a SIR model of the form

$$\begin{cases} S_v'(t) = -\tau_v S_v(t) I_v(t), \\ I_v'(t) = \tau_v S_v(t) I_v(t) - \eta_v I_v(t) + \displaystyle\sum_{e \sim v} \alpha_e^v u_e(t, v) - \overline{\lambda}_v I_v(t), \\ R_v'(t) = \eta_v I_v(t), \end{cases} \tag{2.1}$$

where $\tau_v, \eta_v > 0$ are the intrinsic parameters of the epidemic which may depend on the vertex v. The contribution $-\overline{\lambda}_v I_v(t)$ in the right-hand side of the equation for the infected population traduces the fact that infected individuals can leave the vertex v to incident edges whereas $\sum_{e \sim v} \alpha_e^v u_e(t, v)$ reflects the contribution of incoming infected individuals from incident edges. Here, $e \sim v$ denotes the edges incident to the vertex v and

$$\overline{\lambda}_v := \sum_{e \sim v} \lambda_e^v,$$

such that $\lambda_e^v I_v(t)$ infected individuals leave vertex v to edge e. We have assumed that only the infected population is subject to movement, and we think of S_v being an ambiant population whose movement does not affect its distribution. We recover the standard SIR model (1.1) by considering the trivial graph $\mathcal{G} = (\{v\}, \emptyset)$. Throughout the manuscript, we will assume the following standing hypothesis on the coefficients α_e^v and λ_e^v in (2.1).

Hypothesis 2.1. *For each $(e, v) \in \mathcal{E} \times \mathcal{V}$ we assume that*

$$\alpha_e^v \in (0,1) \quad \textit{and} \quad \lambda_e^v \in (0,1),$$

together with

$$\sum_{e\sim v} \lambda_e^v \in (0,1) \quad \textit{and} \quad \sum_{e\sim v} \alpha_e^v \in (0,1).$$

Next, for each $e \in \mathcal{E}$, we let $d_e > 0$ and we assume that u_e evolves according to

$$\partial_t u_e(t,x) = d_e \partial_x^2 u_e(t,x), \quad t > 0, \quad x \in \overset{\circ}{\Omega}_e. \tag{2.2}$$

Assuming that infected individuals have local diffusion along the edges of the graph is a first approximation, and this can be viewed as a limiting Brownian movement of individuals. We shall come back to this modeling hypothesis later in the manuscript, but possible extensions could be to incorporate nonlocal diffusion or transport terms.

It now remains to model the exchanges of infected individuals at the vertices. Fo each $v \in \mathcal{V}$, we associate an integer $\delta_v \geq 1$ which we refer to as its degree (*i.e.* number of edges incident to the vertex v). We define $\mathbf{u}_v(t) \in \mathbb{R}^{\delta_v}$ as the column vector function

$$\mathbf{u}_v(t) := (u_e(t,v))_{e\sim v},$$

where we recall that $e \sim v$ denotes the edges incident to the vertex v, and thus $u_e(t,v)$ is the corresponding limit value of u_e at $x = v$. Define also $\partial_n \mathbf{u}_v(t) \in \mathbb{R}^{\delta_v}$ as the column vector function

$$\partial_n \mathbf{u}_v(t) := (\partial_n u_e(t,v))_{e\sim v},$$

where $\partial_n u_e(t,v)$ is the outwardly normal derivative of u_e at the vertex v. Our boundary conditions at the vertex v that link (2.1) and (2.2) are described by

$$D_v \partial_n \mathbf{u}_v(t) + K_v \mathbf{u}_v(t) = \Lambda_v \mathbf{I}_v(t), \tag{2.3}$$

where $D_v \in \mathscr{M}_{\delta_v}(\mathbb{R})$ is the diagonal matrix $D_v = \mathrm{diag}[(d_e)_{e\sim v}]$ and $K_v \in \mathscr{M}_{\delta_v}(\mathbb{R})$ whose structure will be specified below. Formally, (2.3) traduces the balance of fluxes of infected individuals at the vertex v, and we will demonstrate this heuristic rigorously by showing in the forthcoming Subsection 2.4 the conservation of total population.

2.2 Assumptions on the connectivity matrices K_v

We now precise the form of the matrix K_v entering in the boundary condition (2.3). Essentially, K_v gathers two contributions. One contribution comes from the exchanges between infected individuals at the vertex with the incoming infected individuals for the incident edges. The second contribution traduces exchanges between edges. Indeed we allow infected individuals to pass from one edge to another one. More precisely, we have that K_v splits into two parts

$$K_v := A_v + N_v,$$

where the matrix $A_v \in \mathscr{M}_{\delta_v}(\mathbb{R})$ is the diagonal matrix $A_v = \mathrm{diag}(\alpha_e^v)_{e\sim v}$ while the matrix $N_v \in \mathscr{M}_{\delta_v}(\mathbb{R})$ is such that the sum of each column is zero. More precisely, if we label by $e \sim v = (e_1, \cdots, e_{\delta_v})$ the edges incident to the vertex v, we have that for all $i = 1, \cdots, \delta_v$

$$(N_v)_{i,i} = \sum_{j\neq i} \nu^v_{e_i,e_j}$$

and for $i \neq j = 1, \cdots, \delta_v$

$$(N_v)_{i,j} = -\nu^v_{e_j,e_i}.$$

In the case $\delta_v = 3$, we get

$$N_v = \begin{pmatrix} \nu^v_{e_1,e_2} + \nu^v_{e_1,e_3} & -\nu^v_{e_2,e_1} & -\nu^v_{e_3,e_1} \\ -\nu^v_{e_1,e_2} & \nu^v_{e_2,e_1} + \nu^v_{e_2,e_3} & -\nu^v_{e_3,e_2} \\ -\nu^v_{e_1,e_3} & -\nu^v_{e_2,e_3} & \nu^v_{e_3,e_1} + \nu^v_{e_3,e_2} \end{pmatrix},$$

see Figure 2 for an illustration in that case.

Furthermore, for the diagonal term we will use the shorthand notation

$$(N_v)_{e,e} = \sum_{e'\neq e} \nu^v_{e,e'}.$$

The fact that $N_v \in \mathscr{M}_{\delta_v}(\mathbb{R})$ is such that the sum of each column is zero precisely traduces the fact that there is the conservation of infected individuals through exchanges between incident edges at each vertex. And, we remark that it implies that the matrix K_v has a strict column diagonal dominance in the sense that for each $i = 1, \cdots, \delta_v$

$$\sum_{j=1}^{\delta_v} (K_v)_{e_i,e_j} = \alpha^v_{e_i} > 0,$$

because of this specific structure of N_v. From now on we also assume that K_v has a diagonal dominance with respect to its lines. This property will be crucial later on in the proof of existence of solutions. As a consequence, we impose the following running assumptions on the matrices K_v.

Hypothesis 2.2. *For each $v \in \mathcal{V}$ and $(e, e') \in \mathcal{E} \times \mathcal{E}$, we assume that*

$$\nu^v_{e,e'} \in [0, 1).$$

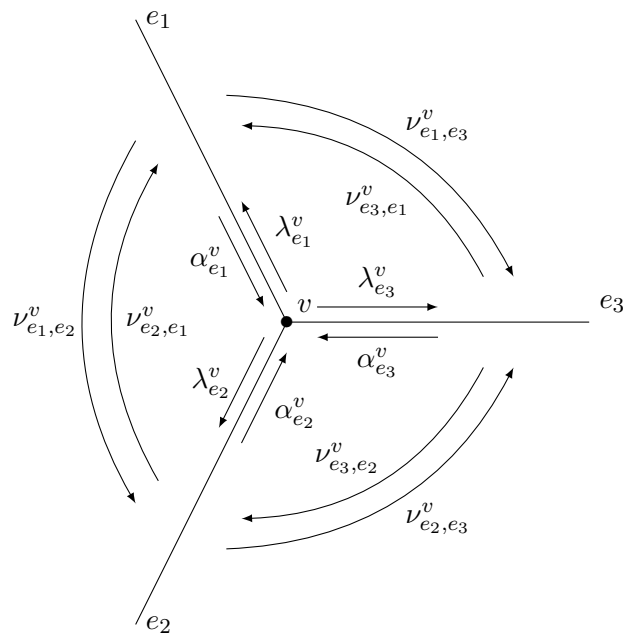

Figure 2: *Schematic illustration of the exchanges at a given vertex v with $\delta_v = 3$.*

Furthermore, we impose that for all $v \in \mathcal{V}$

$$\sum_{e' \neq e} \nu^v_{e',e} < \alpha^v_e + \sum_{e' \neq e} \nu^v_{e,e'},$$

together with

$$(K_v)_{e,e} := \alpha^v_e + \sum_{e' \neq e} \nu^v_{e,e'} \in (0,1),$$

for each $e \sim v$.

Remark 2.3. *If the exchanges between the edges are symmetric, that is for each $v \in \mathcal{V}$ the matrices N_v are symmetric, that is*

$$\nu^v_{e,e'} = \nu^v_{e',e}, \quad \forall (e,e') \in \mathcal{E} \times \mathcal{E},$$

then Hypothesis 2.2 is automatically satisfied.

2.3 Initial configuration

Finally, we complement our coupled PDE-ODE (2.1)-(2.2)-(2.3) with some initial conditions. We assume that at $t = 0$, we have

$$u(t = 0, \cdot) = u^0 \in BC(\mathcal{G}, \mathbb{R}),$$

such that for $e \in \mathcal{E}$,

$$u^0_e(x) \geq 0, \quad x \in \Omega_e.$$

On the other hand, for the ODE system (2.1), we suppose that

$$(S_v(t = 0), I_v(t = 0), R_v(t = 0)) = (S^0_v, I^0_v, 0) \geq \mathbf{0}, \quad \forall v \in \mathcal{V}.$$

We further assume that (2.3) is satisfied at $t = 0$

$$D_v \partial_n \mathbf{u}_v^0 + K_v \mathbf{u}_v^0 = \Lambda_v \mathbf{I}_v^0,$$

with obvious notations $\mathbf{u}_v^0 := (u_e^0(v))_{e\sim v}$ and $\mathbf{I}_v^0 := (I_v^0, \cdots, I_v^0)^{\mathbf{t}}$. Last, we impose that the initial total population of infected individuals is strictly positive,

$$\sum_{v\in\mathcal{V}} I_v^0 > 0,$$

and that susceptible individuals are initially present at each vertex of the graph

$$S_v^0 > 0, \quad \forall v \in \mathcal{V}.$$

This in turn implies that the total population is initially

$$M^0 := \sum_{e\in\mathcal{E}} \int_{\Omega_e} u_e^0(x)\mathrm{d}x + \sum_{v\in\mathcal{V}} \left(S_v^0 + I_v^0\right) > 0.$$

2.4 Conservation of total population

Assuming that there is a solution to $(u, (X_v)_{v\in\mathcal{V}})$ to (2.1)-(2.2)-(2.3), we have that the total mass of the system $M(t)$ defined as

$$M(t) := \sum_{e\in\mathcal{E}} \int_{\Omega_e} u_e(t,x)\mathrm{d}x + \sum_{v\in\mathcal{V}} \left(S_v(t) + I_v(t) + R_v(t)\right)$$

is a conserved quantity and thus independent of t.

To see that, we first remark that

$$\left(S_v'(t) + I_v'(t) + R_v'(t)\right) = \sum_{e\sim v} \alpha_e^v u_e(t,v) - \overline{\lambda}_v I_v(t) = \langle A_v \mathbf{u}_v(t), \mathbf{1}_{\delta_v}\rangle - \langle \Lambda_v \mathbf{I}_v(t), \mathbf{1}_{\delta_v}\rangle$$

with

$$\mathbf{1}_{\delta_v} := (1, \cdots, 1)^{\mathbf{t}} \in \mathbb{R}^{\delta_v},$$

and $\langle \cdot, \cdot \rangle$ is the standard Euclidean inner product on $\mathbb{R}^{\delta_v}$. On the other hand let us define

$$m(t) := \sum_{e\in\mathcal{E}} \int_{\Omega_e} u_e(t,x)\mathrm{d}x,$$

and assume that u is a classical solution of (2.2), which we will prove in the next section, and

compute

$$
\begin{aligned}
m'(t) &= \sum_{e\in\mathcal{E}} \int_{\Omega_e} \partial_t u_e(t,x)\mathrm{d}x = \sum_{e\in\mathcal{E}} d_e \left[\partial_x u_e(t,x)\right]_{\partial\Omega_e} \\
&= \sum_{v\in\mathcal{V}} \langle D_v \partial_n \mathbf{u}_v(t), \mathbf{1}_{\delta_v}\rangle \\
&= \sum_{v\in\mathcal{V}} \langle \Lambda_v \mathbf{I}_v(t) - K_v \mathbf{u}_v(t), \mathbf{1}_{\delta_v}\rangle \\
&= \sum_{v\in\mathcal{V}} \langle \Lambda_v \mathbf{I}_v(t) - A_v \mathbf{u}_v(t), \mathbf{1}_{\delta_v}\rangle - \underbrace{\sum_{v\in\mathcal{V}} \langle N_v \mathbf{u}_v(t), \mathbf{1}_{\delta_v}\rangle}_{=0} \\
&= -\sum_{v\in\mathcal{V}} \left(S_v'(t) + I_v'(t) + R_v'(t)\right).
\end{aligned}
$$

The fact that

$$
\sum_{v\in\mathcal{V}} \langle N_v \mathbf{u}_v(t), \mathbf{1}_{\delta_v}\rangle = 0
$$

is a direct consequence on the specific structure of each matrix N_v and the fact that the sum of each column is zero. We therefore conclude that $M'(t) = 0$ and

$$
\sum_{e\in\mathcal{E}} \int_{\Omega_e} u_e(t,x)\mathrm{d}x + \sum_{v\in\mathcal{V}} \left(S_v(t) + I_v(t) + R_v(t)\right) = M^0, \quad \forall t \geq 0.
$$

Biological interpretation. Our model is thus consistent with the conservation of the total population as it is traditionally the case for SIR model in the case of zero natality/mortality rate. The exchanges between the vertices and the edges exactly compensate each other as is natural.

2.5 Main results and outline of the paper

We now present our main results regarding our model (2.1)-(2.2)-(2.3). At this stage of the presentation, we remain formal and refer to the following sections for precise statements and assumptions.

Main result 1: Existence and uniqueness of classical solutions. We prove in Theorem 1 below that for each well prepared initial condition our model (2.1)-(2.2)-(2.3) admits a unique positive classical solution which is global in time. We remark that the system (2.1)-(2.2)-(2.3) is not standard as it couples a system of PDEs to ODEs at each vertices through inhomogeneous Robin boundary conditions. As a consequence, the existence and uniqueness of classical solutions has to be proved. This analysis is conducted in Section 3.

Main result 2: Long time behavior of the solutions. We fully characterize the long time behavior of the unique solution of our model. More precisely, we prove that the final total population of infected individuals at each vertex, denoted by $\mathcal{I}_v^\infty$, is a well defined quantity: $0 < \mathcal{I}_v^\infty < \infty$ for

$v \in \mathcal{V}$ and $(\mathcal{I}_v^\infty)_{v\in\mathcal{V}}$ are solutions of a system of $c_\mathcal{V}+1$ implicit equations, where $c_\mathcal{V}$ stands for the cardinal of $\mathcal{V}$, which belong to the parametrized submanifold

$$\sum_{v\in\mathcal{V}} \left(S_v^0 e^{-\tau_v \mathcal{I}_v^\infty} + \eta_v \mathcal{I}_v^\infty\right) = M^0,$$

where M^0 is the initial total mass. We refer to Theorem 2 for a precise statement. We also present further qualitative results on the final total configuration $(\mathcal{I}_v^\infty)_{v\in\mathcal{V}}$ in the fully symmetric case where we obtain closed form formula (see Lemma 4.3) and in the case of two vertices where we manage to obtain sharp bounds on the final total populations of infected individuals (see Lemma 4.4). In each case, we manage to relate these quantities to standard basic and effective reproductive number for classical SIR model. The aforementioned results are proved in Section 4.

Main result 3: A mass preserving semi-implicit numerical scheme. We propose and analyze a semi-implicit in time numerical scheme based on finite differences in space which has the property to preserve a *discrete* total mass associated to the discretization. We prove that if the time discretization constant is smaller than a universal constant depending only on the parameters of the system (and not on the space discretization constant) and if N_v is symmetric for each $v \in \mathcal{V}$, then our mass preserving semi-implicit numerical scheme is well-posed and preserves the positivity of the solutions. We refer to Section 5 for a presentation of the numerical scheme and Theorem 3 for a precise statement of our main result.

Main result 4: Numerical results for various types of graphs. We illustrate our theoretical findings with selection of numerical simulations for various types of graphs in Section 6. We respectively study the case of 2 vertices and 1 edge, 3 vertices and 3 edges (closed graph), 4 vertices and 3 edges (star-shape graph) and $N+1$ vertices and N edges with N being arbitrarily large (lattice graph). Most notably, in the last case, we show the propagation of the epidemics across the vertices of the graph in the form of a traveling wave.

3 The Cauchy problem: existence and uniqueness of classical solutions

This section is devoted to the proof of the following main theorem which guarantees that our model is well-posed.

Theorem 1. *For each $(S_v^0, I_v^0) \geq \mathbf{0}$ with $S_v^0 > 0$, $\sum_{v\in\mathcal{V}} I_v^0 > 0$ and $u^0 \in BC(\mathcal{G}, \mathbb{R}^+)$ that satisfy the boundary condition (2.3), there exists a unique positive global solution $(S_v, I_v, R_v) \in \mathscr{C}^1(\mathbb{R}^+, \mathbb{R}^+ \times \mathbb{R}^+ \times \mathbb{R}^+)$ and $u \in \mathscr{C}^{1,2}(\mathbb{R}_*^+ \times \mathcal{G}, \mathbb{R}^+)$.*

The proof of Theorem 1 is divided into two parts. We first prove the existence of positive global classical solutions and then show that such constructed solutions are unique. We look for solutions

that satisfy (2.1)-(2.2)-(2.3) in the classical sense, and we always assume that $(S_v^0, I_v^0) \geq \mathbf{0}$ with $S_v^0 > 0$, $\sum_{v\in\mathcal{V}} I_v^0 > 0$ and $u^0 \in BC(\mathcal{G}, \mathbb{R}^+)$, that is for all $e \in \mathcal{E}$, $u_e^0 \geq 0$ is bounded continuous on Ω_e. We further assume that the initial conditions satisfy the boundary condition (2.3). We remark that the system (2.1)-(2.2)-(2.3) is not standard as it couples a system PDEs to ODEs at each vertices through inhomogeneous Robin boundary conditions. As a consequence, the well-posedness of the Cauchy problem has to be proved.

Remark 3.1. *Our existence and uniqueness result extends trivially in the case that parameters $\tau_v > 0$, $\alpha_e^v \in (0,1)$, $\lambda_e^v \in (0,1)$ and $\nu_{e,e'}^v \in [0,1)$ are continuous functions of time satisfying $\tau_v(t) > 0$, $\alpha_e^v(t) \in (0,1)$, $\lambda_e^v(t) \in (0,1)$ and $\nu_{e,e'}^v(t) \in [0,1)$ together with Hypotheses 2.1-2.2 verified at all times $t > 0$.*

3.1 Existence

In this section, we construct a classical solution to (2.1)-(2.2)-(2.3) through a limiting argument. We will obtain a solution $(u, (X_v)_{v\in\mathcal{V}})$ has the limit of a subsequence of solution $((u^n, (X_v^n)_{v\in\mathcal{V}}))_{n\geq 0}$ of the following problems

$$\begin{cases} \dfrac{\mathrm{d}S_v^n(t)}{\mathrm{d}t} = -\tau_v S_v^n(t) I_v^n(t), \\ \dfrac{\mathrm{d}I_v^n(t)}{\mathrm{d}t} = \tau_v S_v^n(t) I_v^n(t) - (\eta_v + \overline{\lambda}_v) I_v^n(t) + \displaystyle\sum_{e\sim v} \alpha_e^v u_e^{n-1}(t,v), \quad t > 0, \quad \forall v \in \mathcal{V}, \\ \dfrac{\mathrm{d}R_v^n(t)}{\mathrm{d}t} = \eta_v I_v^n(t), \end{cases} \tag{3.1}$$

with

$$D_v \partial_n \mathbf{u}_v^n(t) + K_v \mathbf{u}_v^n(t) = \Lambda_v \mathbf{I}_v^n(t), \quad t > 0, \quad \forall v \in \mathcal{V}, \tag{3.2}$$

and

$$\partial_t u_e^n(t,x) = d_e \partial_x^2 u_e^n(t,x), \quad t > 0, \quad x \in \overset{\circ}{\Omega}_e, \quad \forall e \in \mathcal{E}. \tag{3.3}$$

starting from $u^0 \in BC(\mathcal{G}, \mathbb{R}^+)$ and $(X_v^0)_{v\in\mathcal{V}}$. Note that (3.1)-(3.2)(3.3) is supplemented by the same initial condition $(u^0, (X_v^0)_{v\in\mathcal{V}})$ at each step. We proceed along three main steps.

Step #1: solvability of (3.1)-(3.2)-(3.3). We first show that (3.1)-(3.2)-(3.3) admits a unique solution. It can be done by induction. Assume that at step $n-1$, we have constructed a solution $(u^{n-1}, (X_v^{n-1})_{v\in\mathcal{V}})$ such that for each $t \mapsto u_e^{n-1}(t,v)$ is continuous, then we get the existence of a unique solution of (3.1) which is $\mathscr{C}^1$ in time. Next we solve the system of PDEs (3.3)-(3.2) whose coupling comes from the boundary conditions and owing that now the right-hand side of (3.2) can be seen as given inhomogeneous term of class $\mathscr{C}^1$ in time. As both D_v and K_v are invertible matrices, we get the existence of a classical solution $u^n \in \mathscr{C}^{1,2}$ which then ensures that $t \mapsto u_e^n(t,v)$ is continuous.

Step #2: a priori estimates. Let $0 < T < 1$ be fixed. We first show by a recursive argument that $0 < S_v^n$, $0 \leq I_v^n$, $0 \leq R_v^n$ for each $v \in \mathcal{V}$ and $0 \leq u_e^n$ for each $e \in \mathcal{E}$. It is trivial at $n = 0$. Let assume that is it true at $n-1$. We start from (3.1) and a direct integration gives

$$
\begin{aligned}
S_v^n(t) &= S_v^0 e^{-\tau_v \int_0^t I_v^n(s)\mathrm{d}s} > 0, \\
I_v^n(t) &= I_v^0 e^{-(\eta_v+\overline{\lambda}_v)t+\int_0^t S_v^n(s)\mathrm{d}s} + \sum_{e\sim v} \alpha_e^v \int_0^t e^{-(\eta_v+\overline{\lambda}_v)(t-s)+\int_s^t S_v^n(\tau)\mathrm{d}\tau} u_e^{n-1}(s,v)\mathrm{d}s \geq 0, \\
R_v^n(t) &= \eta_v \int_0^t I_v^n(s)\mathrm{d}s \geq 0.
\end{aligned}
$$

Now owing that $0 \leq I_v^n$ for each $v \in \mathcal{V}$, the maximum principle implies that $u_e^n \geq 0$ for each $e \in \mathcal{E}$. Assume by contradiction that $e_* \in \mathcal{E}$ is the component which reaches a negative minimum, namely $u_{e_*}^n(t_*, x_*) = -\delta < 0$ with $u_{e_*}^n(t,x) > -\delta$ for $t < t_*$ and $x \in \Omega_{e_*}$ and for each $e \neq e_*$ we have $u_e^n(t,x) > -\delta$ for $t \leq t_*$ and $x \in \Omega_e$. We know that $x_* \in \partial\Omega_{e_*}$ and let denote $v_* = x_* \in \mathcal{V}$ the vertex where this occurs. The Hopf lemma implies that $\partial_n u_{e_*}^n(t_*, v_*) < 0$. Inspecting the boundary condition (3.2) at v_*, we obtain that

$$
d_{e_*}\partial_n u_{e_*}^n(t_*,v_*) + \alpha_{e_*}^{v_*} u_{e_*}^n(t_*,v_*) + \left(\sum_{e\sim e_*} \nu_{e_*,e}^{v_*}\right) u_{e_*}^n(t_*,v_*) - \sum_{e\sim e_*} \nu_{e,e_*}^{v_*} u_e^n(t_*,v_*) = \lambda_{e_*}^{v_*} I_{v_*}^n(t),
$$

which writes

$$
0 > d_{e_*}\partial_n u_{e_*}^n(t_*,v_*) + \delta\left(\sum_{e\sim e_*} \nu_{e,e_*}^{v_*} - \alpha_{e_*}^{v_*} - \sum_{e\sim e_*} \nu_{e_*,e}^{v_*}\right) - \sum_{e\sim e_*} \nu_{e,e_*}^{v_*}(\delta + u_e^n(t_*,v_*)) = \lambda_{e_*}^{v_*} I_{v_*}^n(t) \geq 0,
$$

and leads to a contradiction. Here we have used the fact that

$$
\sum_{e\sim e_*} \nu_{e,e_*}^{v_*} \leq \alpha_{e_*}^{v_*} + \sum_{e\sim e_*} \nu_{e_*,e}^{v_*},
$$

from Hypothesis 2.2 on the matrices $(K_v)_{v\in\mathcal{V}}$.

Next, from the positivity of solutions, we obtain some uniform L^∞ bounds. More precisely, we claim that there exists a constant $K > 0$ depending only on $(T, I_v^0, S_v^0, \|u^0\|_\infty)$ such that

$$
0 \leq S_v^n(t), I_v^n(t), R_v^n(t) \leq K, \text{ and } \left|\frac{\mathrm{d}S_v^n(t)}{\mathrm{d}t}\right|, \left|\frac{\mathrm{d}I_v^n(t)}{\mathrm{d}t}\right|, \left|\frac{\mathrm{d}R_v^n(t)}{\mathrm{d}t}\right| \leq K \quad 0 < t \leq T,
$$

and

$$
0 \leq u_e^n(t,x) \leq K, \quad 0 < t \leq T, \quad x \in \Omega_e.
$$

First, using (3.1) we obtain that

$$
\frac{\mathrm{d}S_v^n(t)}{\mathrm{d}t} + \frac{\mathrm{d}I_v^n(t)}{\mathrm{d}t} + \frac{\mathrm{d}R_v^n(t)}{\mathrm{d}t} = -\overline{\lambda}_v I_v^n(t) + \sum_{e\sim v} \alpha_e^v u_e^{n-1}(t,v),
$$

which gives that

$$
0 \leq S_v^n(t) + I_v^n(t) + R_v^n(t) \leq S_v^0 + I_v^0 + T\|u^{n-1}\|_\infty, \quad 0 < t \leq T,
$$

together with

$$\left|\frac{\mathrm{d}S_v^n(t)}{\mathrm{d}t}\right|, \left|\frac{\mathrm{d}I_v^n(t)}{\mathrm{d}t}\right|, \left|\frac{\mathrm{d}R_v^n(t)}{\mathrm{d}t}\right| \leq C\|u^{n-1}\|_\infty(1+T+T^2\|u^{n-1}\|_\infty) \quad 0<t\leq T,$$

which in turn implies that

$$\|u^n\|_\infty \leq \tilde{C}T\|u^{n-1}\|_\infty(1+T+T^2\|u^{n-1}\|_\infty),$$

for $C, \tilde{C} > 0$ only depend on the initial condition $(u^0, (X_v^0)_{v\in\mathcal{V}})$ and the parameters of the system. We now claim that by induction, we have for all $0 < t \leq T$,

$$0 \leq S_v^n(t) + I_v^n(t) + R_v^n(t) \leq \hat{C}\sum_{p=0}^{a_n} T^p,$$

$$\left|\frac{\mathrm{d}S_v^n(t)}{\mathrm{d}t}\right|, \left|\frac{\mathrm{d}I_v^n(t)}{\mathrm{d}t}\right|, \left|\frac{\mathrm{d}R_v^n(t)}{\mathrm{d}t}\right| \leq \hat{C}\sum_{p=0}^{2a_n} T^p,$$

$$\|u^n\|_\infty \leq \hat{C}\sum_{p=0}^{2a_n} T^{p+1},$$

with $a_n = 2 + 2a_{n-1}$ for $n \geq 2$ and $a_1 = 1$ for some $\hat{C} > 0$ only depending on $(u^0, (X_v^0)_{v\in\mathcal{V}})$. As $0 < T < 1$, we get that

$$0 \leq S_v^n(t) + I_v^n(t) + R_v^n(t) \leq \hat{C}_T, \quad 0 < t \leq T,$$

together with

$$\|u^n\|_\infty, \left|\frac{\mathrm{d}S_v^n(t)}{\mathrm{d}t}\right|, \left|\frac{\mathrm{d}I_v^n(t)}{\mathrm{d}t}\right|, \left|\frac{\mathrm{d}R_v^n(t)}{\mathrm{d}t}\right| \leq \hat{C}_T,$$

for some constant $\hat{C}_T > 0$ depending on $(T, u^0, (X_v^0)_{v\in\mathcal{V}})$.

Step #3: existence of a solution. Parabolic Schauder estimates give that the time derivative and the space derivatives up to order 2 of u^n are uniformly Hölder continuous in compact sets. As a consequence, we can use the Arzela-Ascoli theorem to show that $(u^n, (X_v^n)_{v\in\mathcal{V}})$ converges (up to sequences) toward $(u, (X_v)_{v\in\mathcal{V}})$ in $\mathcal{C}^{1,2}_{loc}((0,T)\times\mathcal{G}) \times \mathcal{C}^1_{loc}((0,T)) \times \mathcal{C}^1_{loc}((0,T)) \times \mathcal{C}^1_{loc}((0,T))$. Passing to the limit $n \to +\infty$ in (3.1)-(3.2)-(3.3) we get that $(u, (X_v)_{v\in\mathcal{V}})$ satisfies (2.1)-(2.2) subject to boundary conditions (2.3).

As a by product of the proof we get that for the just constructed solution $(u, (X_v)_{v\in\mathcal{V}})$ we have the uniform bounds:

$$0 < S_v(t) \leq S_v^0, \quad 0 < t \leq T, \quad v \in \mathcal{V},$$

and

$$0 \leq I_v(t), R_v(t) \quad 0 < t \leq T,$$

together with

$$0 \leq u_e(t,x), \quad 0 < t \leq T, \quad x \in \Omega_e, \quad e \in \mathcal{E}.$$

The fact that $I_v(t) \geq 0$ implies thanks to the strong maximum principle that in fact

$$0 < u_e(t,x), \quad 0 < t \leq T, \quad x \in \Omega_e, \quad e \in \mathcal{E},$$

which in turn gives that $I_v(t) > 0$ for each $v \in \mathcal{V}$ since

$$I_v^n(t) = I_v^0 e^{-(\eta_v + \overline{\lambda}_v)t + \int_0^t S_v^n(s)\mathrm{d}s} + \sum_{e \sim v} \alpha_e^v \int_0^t e^{-(\eta_v + \overline{\lambda}_v)(t-s) + \int_s^t S_v^n(\tau)\mathrm{d}\tau} u_e^{n-1}(s,v)\mathrm{d}s > 0.$$

Finally, we use the conservation of mass which tells us that

$$\sum_{e \in \mathcal{E}} \int_{\Omega_e} u_e(t,x)\mathrm{d}x + \sum_{v \in \mathcal{V}} (S_v(t) + I_v(t) + R_v(t)) = M^0 > 0, \quad 0 < t \leq T,$$

such that both $I_v(t)$ and $R_v(t)$ are uniformly bounded in time, together with their derivatives. This also implies that there exists a constant $M > 0$, depending only $(u^0, (X_v^0)_{v \in \mathcal{V}})$ such that

$$0 < u(t,x) \leq M, \quad 0 < t \leq M, \quad x \in \Omega_e.$$

Using again parabolic regularity, we obtain the solution $(u, (X_v)_{v \in \mathcal{V}})$ is global in time and satisfies (2.1)-(2.2)-(2.3) in the classical sense.

3.2 Uniqueness

Let assume that $(u, (X_v)_{v \in \mathcal{V}})$ and $(\tilde{u}, (\tilde{X}_v)_{v \in \mathcal{V}})$ are two classical solutions to (2.2)-(2.3)-(2.1) starting from the same initial datum $(u^0, (X_v^0)_{v \in \mathcal{V}})$. We denote $(\hat{u}, (\hat{X}_v)_{v \in \mathcal{V}})$ where for each $e \in \mathcal{E}$

$$\hat{u}_e = u_e - \tilde{u}_e,$$

and each $v \in \mathcal{V}$

$$\hat{X}_v = (\hat{S}_v, \hat{I}_v, \hat{R}_v) = (S_v - \tilde{S}_v, I_v - \tilde{I}_v, R_v - \tilde{R}_v).$$

By linearity, we get that for $e \in \mathcal{E}$

$$\partial_t \hat{u}_e = d_e \partial_x^2 \hat{u}_e, \quad t > 0, \quad x \in \overset{\circ}{\Omega}_e,$$

together with

$$D_v \partial_n \hat{\mathbf{u}}_v(t) + K_v \hat{\mathbf{u}}_v(t) = \Lambda_v \hat{\mathbf{I}}_v(t), \quad t > 0, \quad v \in \mathcal{V}.$$

On the other, one computes that $\hat{X}_v$ satisfies for each $v \in \mathcal{V}$

$$\begin{cases} \hat{S}_v'(t) = -\tau_v \left(S_v(t)\hat{I}_v(t) + \hat{S}_v(t)\tilde{I}_v(t) \right), \\ \hat{I}_v'(t) = \tau_v \left(S_v(t)\hat{I}_v(t) + \hat{S}_v(t)\tilde{I}_v(t) \right) - \eta_v \hat{I}_v(t) + \sum_{e \sim v} \alpha_e^v \hat{u}_e(t,v) - \overline{\lambda}_v \hat{I}_v(t), \\ \hat{R}_v'(t) = \eta_v \hat{I}_v(t), \end{cases}$$

We define the energy

$$\mathscr{E}(t) := \frac{1}{2}\sum_{e\in\mathcal{E}}\int_{\Omega_e}(\hat{u}_e(t,x))^2\,\mathrm{d}x + \frac{1}{2}\sum_{v\in\mathcal{V}}\left(\hat{S}_v(t)^2+\hat{I}_v(t)^2+\hat{R}_v(t)^2\right),$$

and note that $\mathscr{E}(0)=0$ by definition. Next, differentiating $\mathscr{E}(t)$, we obtain

$$\begin{aligned}\mathscr{E}'(t) &= \sum_{e\in\mathcal{E}}\int_{\Omega_e}\hat{u}_e(t,x)\partial_t\hat{u}_e(t,x)\mathrm{d}x + \sum_{v\in\mathcal{V}}\left(\hat{S}_v(t)\hat{S}_v'(t)+\hat{I}_v(t)\hat{I}_v'(t)+\hat{R}_v(t)\hat{R}_v'(t)\right)\\ &:= \mathscr{E}_u(t)+\mathscr{E}_X(t).\end{aligned}$$

On the one hand, we have

$$\begin{aligned}\mathscr{E}_u(t) &= \sum_{e\in\mathcal{E}}\int_{\Omega_e}\hat{u}_e(t,x)\partial_t\hat{u}_e(t,x)\mathrm{d}x = \sum_{e\in\mathcal{E}}d_e\int_{\Omega_e}\hat{u}_e(t,x)\partial_x^2\hat{u}_e(t,x)\mathrm{d}x\\ &= -\sum_{e\in\mathcal{E}}d_e\int_{\Omega_e}(\partial_x\hat{u}_e(t,x))^2\,\mathrm{d}x + \sum_{e\in\mathcal{E}}d_e\left[\hat{u}_e(t,x)\partial_t\hat{u}_e(t,x)\right]_{\partial\Omega_e}\\ &\le \sum_{v\in\mathcal{V}}\langle D_v\partial_n\hat{\mathbf{u}}_v(t),\hat{\mathbf{u}}_v(t)\rangle\\ &= \sum_{v\in\mathcal{V}}\langle\Lambda_v\hat{\mathbf{I}}_v(t)-K_v\hat{\mathbf{u}}_v(t),\hat{\mathbf{u}}_v(t)\rangle\\ &= \sum_{v\in\mathcal{V}}\langle\Lambda_v\hat{\mathbf{I}}_v(t)-A_v\hat{\mathbf{u}}_v(t),\hat{\mathbf{u}}_v(t)\rangle - \sum_{v\in\mathcal{V}}\langle N_v\hat{\mathbf{u}}_v(t),\hat{\mathbf{u}}_v(t)\rangle\\ &\le \sum_{v\in\mathcal{V}}\langle\Lambda_v\hat{\mathbf{I}}_v(t)-A_v\hat{\mathbf{u}}_v(t),\hat{\mathbf{u}}_v(t)\rangle,\end{aligned}$$

as N_v is symmetric positive. On the other hand, we compute

$$\begin{aligned}\mathscr{E}_u(t) &= \sum_{v\in\mathcal{V}}\left(\hat{S}_v(t)\hat{S}_v'(t)+\hat{I}_v(t)\hat{I}_v'(t)+\hat{R}_v(t)\hat{R}_v'(t)\right)\\ &= \sum_{v\in\mathcal{V}}\tau_v\left(S_v(t)\hat{I}_v(t)\hat{S}_v(t)+\hat{S}_v(t)^2\tilde{I}_v(t)+S_v(t)\hat{I}_v(t)^2+\hat{S}_v(t)\tilde{I}_v(t)\hat{I}_v(t)\right)\\ &\quad -\sum_{v\in\mathcal{V}}\eta_v\hat{I}_v(t)^2-\sum_{v\in\mathcal{V}}\overline{\lambda}_v\hat{I}_v(t)^2+\sum_{v\in\mathcal{V}}\hat{I}_v(t)\sum_{e\sim v}\alpha_e^v\hat{u}_e(t,v)+\sum_{v\in\mathcal{V}}\eta_v\hat{R}_v(t)\hat{I}_v(t)\\ &\le C\mathscr{E}(t)+\sum_{v\in\mathcal{V}}\hat{I}_v(t)\sum_{e\sim v}\alpha_e^v\hat{u}_e(t,v),\end{aligned}$$

where $C>0$ is some large positive constant. Next, we see that

$$\sum_{v\in\mathcal{V}}\hat{I}_v(t)\sum_{e\sim v}\alpha_e^v\hat{u}_e(t,v) = \sum_{v\in\mathcal{V}}\langle\hat{\mathbf{I}}_v(t),A_v\hat{\mathbf{u}}_v(t)\rangle,$$

such that we obtain

$$\mathscr{E}'(t)\le C\mathscr{E}(t)+\sum_{v\in\mathcal{V}}\langle\Lambda_v\hat{\mathbf{I}}_v(t)-A_v\hat{\mathbf{u}}_v(t),\hat{\mathbf{u}}_v(t)\rangle+\sum_{v\in\mathcal{V}}\langle\hat{\mathbf{I}}_v(t),A_v\hat{\mathbf{u}}_v(t)\rangle.$$

Next, if we denote $\hat{\mathbf{w}}_v(t) := \frac{1}{2}A_v^{-1/2}\left(\Lambda_v + A_v\right)\hat{\mathbf{I}}_v(t) - A_v^{1/2}\hat{\mathbf{u}}_v(t)$, we compute

$$\begin{aligned}
0 \leq \sum_{v\in\mathcal{V}} \langle \hat{\mathbf{w}}_v(t), \hat{\mathbf{w}}_v(t)\rangle &= \frac{1}{4}\sum_{v\in\mathcal{V}} \langle A_v^{-1}\left(\Lambda_v + A_v\right)^2 \hat{\mathbf{I}}_v(t), \hat{\mathbf{I}}_v(t)\rangle - \sum_{v\in\mathcal{V}} \langle \left(\Lambda_v + A_v\right)\hat{\mathbf{I}}_v(t), \hat{\mathbf{u}}_v(t)\rangle \\
&\quad + \sum_{v\in\mathcal{V}} \langle A_v\hat{\mathbf{u}}_v(t), \hat{\mathbf{u}}_v(t)\rangle \\
&= \frac{1}{4}\sum_{v\in\mathcal{V}} \langle A_v^{-1}\left(\Lambda_v + A_v\right)^2 \hat{\mathbf{I}}_v(t), \hat{\mathbf{I}}_v(t)\rangle - \sum_{v\in\mathcal{V}} \langle \Lambda_v\hat{\mathbf{I}}_v(t) - A_v\hat{\mathbf{u}}_v(t), \hat{\mathbf{u}}_v(t)\rangle \\
&\quad - \sum_{v\in\mathcal{V}} \langle \hat{\mathbf{I}}_v(t), A_v\hat{\mathbf{u}}_v(t)\rangle.
\end{aligned}$$

As a consequence, we get

$$\begin{aligned}
\mathscr{E}'(t) &\leq C\mathscr{E}(t) + \frac{1}{4}\sum_{v\in\mathcal{V}} \langle A_v^{-1}\left(\Lambda_v + A_v\right)^2 \hat{\mathbf{I}}_v(t), \hat{\mathbf{I}}_v(t)\rangle - \sum_{v\in\mathcal{V}} \langle \hat{\mathbf{w}}_v(t), \hat{\mathbf{w}}_v(t)\rangle \\
&\leq \tilde{C}\mathscr{E}(t),
\end{aligned}$$

for some $\tilde{C} > 0$ and we conclude that $\mathscr{E}(t) = 0$ for all time which then implies that $\hat{u} = 0$ and $\hat{X}_v = 0$.

4 Long-time behavior of the solutions

Throughout this section, we denote by $(u, (X_v)_{v\in\mathcal{V}})$ the unique positive bounded classical solution of the Cauchy problem (2.1)-(2.2)-(2.3) as given by Theorem 1 and which further satisfies the conservation of total population, namely

$$\sum_{e\in\mathcal{E}} \int_{\Omega_e} u_e(t,x)\mathrm{d}x + \sum_{v\in\mathcal{V}} \left(S_v(t) + I_v(t) + R_v(t)\right) = M^0 > 0, \quad \forall t > 0.$$

4.1 Final total populations: general results

As $0 < S_v(t) < S_v^0$ and $S_v(t)$ is strictly decreasing, it asymptotically converges towards a limit that we denote

$$S_v^\infty := \lim_{t\to+\infty} S_v(t), \quad v \in \mathcal{V}.$$

Furthermore, as $R_v(t)$ is strictly increasing and uniformly bounded, it asymptotically converges towards a limit that is denoted

$$0 < R_v^\infty := \lim_{t\to+\infty} R_v(t) < \infty, \quad v \in \mathcal{V}.$$

But as for each $t > 0$

$$R_v(t) = \eta_v \int_0^t I_v(s)\mathrm{d}s,$$

this implies that

$$\mathcal{I}_v(t) := \int_0^t I_v(s)\mathrm{d}s \longrightarrow \mathcal{I}_v^\infty = \frac{R_v^\infty}{\eta_v} < \infty \text{ as } t \to +\infty,$$

which in turn proves that

$$I_v^\infty = \lim_{t\to+\infty} I_v(t) = 0.$$

If one recall the notation $m(t)$ for the total population on the edges then we have

$$m(t) = \sum_{e\in\mathcal{E}} \int_{\Omega_e} u_e(t,x)\mathrm{d}x,$$

and it verifies

$$\sum_{v\in\mathcal{V}} (S_v(t) + I_v(t) + R_v(t)) + m(t) = \sum_{v\in\mathcal{V}} \left(S_v^0 + I_v^0\right) + \sum_{e\in\mathcal{E}} \int_{\Omega_e} u_e^0(x)\mathrm{d}x.$$

The above computations shows that $m(t)$ has a limit as $t \longrightarrow +\infty$, that we denote m_∞ and which satisfies

$$\sum_{v\in\mathcal{V}} (S_v^\infty + R_v^\infty) + m_\infty = \sum_{v\in\mathcal{V}} \left(S_v^0 + I_v^0\right) + \sum_{e\in\mathcal{E}} \int_{\Omega_e} u_e^0(x)\mathrm{d}x. \tag{4.1}$$

We shall also keep in mind that

$$S_v^\infty = S_v^0 e^{-\tau_v \mathcal{I}_v^\infty} = S_v^0 e^{-\frac{\tau_v}{\eta_v} R_v^\infty}, \text{ or } R_v^\infty = -\frac{\eta_v}{\tau_v} \ln \frac{S_v^\infty}{S_v^0}, \quad v \in \mathcal{V}$$

And so if we introduce the function $\Psi_v(x) := x - \frac{\eta_v}{\tau_v} \ln x$, then the above conservation of mass can be written as

$$\sum_{v\in\mathcal{V}} \Psi_v(S_v^\infty) + m_\infty = \sum_{v\in\mathcal{V}} \left(I_v^0 + \Psi_v(S_v^0)\right) + \sum_{e\in\mathcal{E}} \int_{\Omega_e} u_e^0(x)\mathrm{d}x.$$

On the other, one can compute that

$$\frac{\mathrm{d}m(t)}{\mathrm{d}t} = \sum_{v\in\mathcal{V}} \overline{\lambda}_v I_v(t) - \sum_{v\in\mathcal{V}} \langle A_v \mathbf{u}_v(t), \mathbf{1}_{\delta_v}\rangle,$$

such that

$$m(t) + \sum_{v\in\mathcal{V}} \int_0^t \langle A_v \mathbf{u}_v(s), \mathbf{1}_{\delta_v}\rangle \mathrm{d}s = \sum_{e\in\mathcal{E}} \int_{\Omega_e} u_e^0(x)\mathrm{d}x + \sum_{v\in\mathcal{V}} \overline{\lambda}_v \mathcal{I}_v(t).$$

Now, as $m(t)$ and each $\mathcal{I}_v(t)$ are convergent we deduce that all $\int_0^t \mathbf{u}_v(s)\mathrm{d}s$ are also convergent so that

$$m_\infty + \sum_{v\in\mathcal{V}} \int_0^\infty \langle A_v \mathbf{u}_v(s), \mathbf{1}_{\delta_v}\rangle \mathrm{d}s = \sum_{e\in\mathcal{E}} \int_{\Omega_e} u_e^0(x)\mathrm{d}x + \sum_{v\in\mathcal{V}} \overline{\lambda}_v \mathcal{I}_v^\infty, \tag{4.2}$$

and

$$\int_0^\infty \mathbf{u}_v(s)\mathrm{d}s < \infty, \quad v \in \mathcal{V},$$

which proves that

$$\mathbf{u}_v(t) \longrightarrow 0 \text{ as } t \to +\infty, \quad v \in \mathcal{V}.$$

And the boundary conditions imply that

$$\partial_n \mathbf{u}_v(t) \longrightarrow 0 \text{ as } t \to +\infty, \quad v \in \mathcal{V}.$$

Next, we define the sequence of functions $u_e^n(t,x) = u_e(t+n,x)$ for each $e \in \mathcal{E}$ and $X_v^n(t) = X_v(t+n)$ for each $v \in \mathcal{V}$ which are uniformly bounded such that one can extract a convergent subsequence. On the one hand we have that $\lim_{n\to\infty} X_v^n(t) = X_v^\infty = (S_v^\infty, 0, R_v^\infty)$ and on the other if $u_e^\infty(t,x) = \lim_{n\to\infty} u_e^n(t,x)$ it is solution of

$$\partial_t u_e^\infty(t,x) = d_e \partial_x^2 u_e^\infty(t,x),$$

with the boundary conditions

$$\partial_n \mathbf{u}_v^\infty(t) = \mathbf{u}_v^\infty(t) = \mathbf{0}_{\delta_v}, \quad v \in \mathcal{V}.$$

This then shows that $u_e^\infty(t,x) = 0$, $t > 0$ and $x \in \overset{\circ}{\Omega}_e$ for each $e \in \mathcal{E}$. As there is unicity of the limit, we deduce that

$$\lim_{t\to+\infty} u_e(t,x) = 0, \quad e \in \mathcal{E}.$$

From which we also get that $m_\infty = 0$ and that

$$\sum_{v\in\mathcal{V}} \Psi_v(S_v^\infty) = \sum_{v\in\mathcal{V}} \left(I_v^0 + \Psi_v(S_v^0)\right) + \sum_{e\in\mathcal{E}} \int_{\Omega_e} u_e^0(x)\mathrm{d}x.$$

This implies that each $\Psi_v(S_v^\infty)$ is bounded, we get that $S_v^\infty > 0$ for all $v \in \mathcal{V}$.

We also get from (4.2), that

$$\sum_{v\in\mathcal{V}} \int_0^\infty \langle A_v \mathbf{u}_v(s), \mathbf{1}_{\delta_v}\rangle \mathrm{d}s = \sum_{e\in\mathcal{E}} \int_{\Omega_e} u_e^0(x)\mathrm{d}x + \sum_{v\in\mathcal{V}} \overline{\lambda}_v \mathcal{I}_v^\infty.$$

Finally, we use the fact that

$$\frac{\mathrm{d}I_v(t)}{\mathrm{d}t} + \frac{\mathrm{d}S_v(t)}{\mathrm{d}t} - \frac{\eta_v + \overline{\lambda}_v}{\tau_v} \frac{\mathrm{d}\ln S_v(t)}{\mathrm{d}t} = \sum_{e\sim v} \alpha_e^v u_e(t,v), \quad v \in \mathcal{V},$$

to obtain that

$$I_v(t) + S_v(t) - \frac{\eta_v + \overline{\lambda}_v}{\tau_v} \ln S_v(t) - I_v^0 - S_v^0 + \frac{\eta_v + \overline{\lambda}_v}{\tau_v} \ln S_v^0 = \sum_{e\sim v} \alpha_e^v \int_0^t u_e(s,v)\mathrm{d}s, \quad v \in \mathcal{V}.$$

As a consequence, the final total populations of infected individuals at each vertices satisfy the following scalar differential equation

$$\frac{\mathrm{d}\mathcal{I}_v(t)}{\mathrm{d}t} = S_v^0 \left(1 - e^{-\tau_v \mathcal{I}_v(t)}\right) - \eta_v \mathcal{I}_v(t) + I_v^0 + \sum_{e\sim v} \alpha_e^v \int_0^t u_e(s,v)\mathrm{d}s - \overline{\lambda}_v \mathcal{I}_v(t), \quad v \in \mathcal{V}. \tag{4.3}$$

Passing to the limit as $t \to +\infty$, we get

$$0 = S_v^0 \left(1 - e^{-\tau_v \mathcal{I}_v^\infty}\right) - \eta_v \mathcal{I}_v^\infty + I_v^0 + \sum_{e\sim v} \alpha_e^v \int_0^\infty u_e(s,v)\mathrm{d}s - \overline{\lambda}_v \mathcal{I}_v^\infty, \quad v \in \mathcal{V}.$$

To summarize, we have proved the following result.

Theorem 2. *For each $(S_v^0, I_v^0) \geq \mathbf{0}$ with $S_v^0 > 0$, $\sum_{v\in\mathcal{V}} I_v^0 > 0$ and $u^0 \in BC(\mathcal{G}, \mathbb{R}^+)$ that satisfy the boundary condition (2.3), the long time behavior of the unique corresponding solution $(u, (X_v)_{v\in\mathcal{V}})$ is given by*

$$\lim_{t\to+\infty} u_e(t,x) = 0, \quad x \in \Omega_e, \quad e \in \mathcal{E}, \quad \text{with} \quad \int_0^\infty u_e(s,v)\mathrm{d}s < +\infty, \quad (v,e) \in \mathcal{G},$$

and

$$\lim_{t\to+\infty} (S_v(t), I_v(t), R_v(t)) = \left(S_v^0 e^{-\tau_v \mathcal{I}_v^\infty}, 0, \eta_v \mathcal{I}_v^\infty\right), \quad v \in \mathcal{V}, \tag{4.4}$$

where the final total populations of infected individuals $0 < \mathcal{I}_v^\infty < \infty$ at each vertices $v \in \mathcal{V}$ are solutions of the system

$$\begin{cases} S_v^0 e^{-\tau_v \mathcal{I}_v^\infty} + \eta_v \mathcal{I}_v^\infty = I_v^0 + S_v^0 + \displaystyle\sum_{e\sim v} \alpha_e^v \int_0^\infty u_e(s,v)\mathrm{d}s - \overline{\lambda}_v \mathcal{I}_v^\infty, \quad v \in \mathcal{V}, \\ \displaystyle\sum_{v\in\mathcal{V}} \int_0^\infty \langle A_v \mathbf{u}_v(s), \mathbf{1}_{\delta_v}\rangle \mathrm{d}s = \sum_{e\in\mathcal{E}} \int_{\Omega_e} u_e^0(x)\mathrm{d}x + \sum_{v\in\mathcal{V}} \overline{\lambda}_v \mathcal{I}_v^\infty. \end{cases} \tag{4.5}$$

As a consequence, $(\mathcal{I}_v^\infty)_{v\in\mathcal{V}}$ belongs to the parametrized submanifold given by

$$\sum_{v\in\mathcal{V}} \left(S_v^0 e^{-\tau_v \mathcal{I}_v^\infty} + \eta_v \mathcal{I}_v^\infty\right) = M^0. \tag{4.6}$$

Remark 4.1. *Equivalently, $(S_v^\infty)_{v\in\mathcal{V}}$ belongs to the parametrized submanifold given by*

$$\sum_{v\in\mathcal{V}} \left(S_v^\infty - \frac{\eta_v}{\tau_v} \log\left(S_v^\infty\right) + \frac{\eta_v}{\tau_v} \log\left(S_v^0\right)\right) = M^0, \tag{4.7}$$

and $(R_v^\infty)_{v\in\mathcal{V}}$ belongs to the parametrized submanifold given by

$$\sum_{v\in\mathcal{V}} \left(S_v^0 \exp(-\tau_v/\eta_v\, R_v^\infty) + R_v^\infty\right) = M^0. \tag{4.8}$$

The equations (4.6), (4.7), and (4.8) also read $\sum_{v\in\mathcal{V}} (S_v^\infty + R_v^\infty) = M^0$, which is nothing but (4.1) since we have proved that $m_\infty = 0$.

Remark 4.2. *If we assume that $\tau = \tau_v > 0$ and $\eta = \eta_v > 0$ are independent of $v \in \mathcal{V}$ and let $\widetilde{S_v} = \tau/\eta\, S_v$, $\widetilde{R_v^\infty} = \exp(-\tau/\eta\, R_v^\infty)$ and $\widetilde{\mathcal{I}_v^\infty} = \exp(-\tau \mathcal{I}_v^\infty)$. Then, equations (4.6), (4.7), and (4.8) are respectively equivalent to*

$$\prod_{v\in\mathcal{V}} \exp\left(\widetilde{S_v^\infty}\right) \frac{\widetilde{S_v^0}}{\widetilde{S_v^\infty}} = \exp\left(\frac{\tau}{\eta} M^0\right),$$

$$\prod_{v\in\mathcal{V}} \frac{\exp\left(\widetilde{S_v^0}\widetilde{R_v^\infty}\right)}{\widetilde{R_v^\infty}} = \exp\left(\frac{\tau}{\eta} M^0\right),$$

and

$$\prod_{v\in\mathcal{V}} \frac{\exp\left(\widetilde{S_v^0}\widetilde{\mathcal{I}_v^\infty}\right)}{\widetilde{\mathcal{I}_v^\infty}} = \exp\left(\frac{\tau}{\eta} M^0\right).$$

The common right hand side features $\frac{\tau}{\eta} M^0$ that is nothing but the traditional basic reproductive number $\mathscr{R}_0$.

4.2 Final total populations of infected individuals: further properties

The aim of this section is to present further qualitative results on the final total configuration $(\mathcal{I}_v^\infty)_{v\in\mathcal{V}}$ in the fully symmetric case where one can obtain closed form formula and in the case of two vertices where we manage to obtain sharp bounds on the final total populations of infected individuals. In each case, we manage to relate these quantities to standard basic and effective reproductive number for classical SIR model [10].

Fully symmetric case. We assume that the length ℓ_e of every edge $e \in \mathcal{E}$ is equal to a reference length ℓ. For every $e \in \mathcal{E}$, the diffusion coefficient d_e is equal to d. We moreover suppose that for every vertex $v \in \mathcal{V}$, $S_v^0 = S^0$, $I_v^0 = I^0$ and $R_v^0 = R^0$. We also assume that $\tau = \tau_v > 0$ and $\eta = \eta_v > 0$ are independent of $v \in \mathcal{V}$. In the same spirit, $\lambda_e^v = \lambda$ and $\alpha_e^v = \alpha$ for every $e \in \mathcal{E}$ and $v \in \mathcal{V}$. We also assume $\nu_{e_i,e_j}^v = \nu$ for every edges incident to the vertex v. Finally, the components u_e^0 of initial condition on each edges $e \in \mathcal{E}$ are supposed to be even with respect to the center of the interval $\Omega_e = [0, \ell]$. Thanks to all these assumptions, $\mathcal{I}_v^\infty$ does not depend on the vertex $v \in \mathcal{V}$ and we set $\mathcal{I}_v^\infty = \mathcal{I}^\infty$. Let us recall the notation $c_\mathcal{V}$ for the cardinal of the set $\mathcal{V}$. The parametrized submanifold given by (4.6) becomes

$$S^\infty + R^\infty = S^0 e^{-\tau\mathcal{I}^\infty} + \eta\mathcal{I}^\infty = \widetilde{M^0},$$

where $\widetilde{M^0} = M^0/c_\mathcal{V}$. We can transform this relation as

$$S^0 e^{-\tau\mathcal{I}^\infty} + \frac{\eta}{\tau}\tau\mathcal{I}^\infty - \widetilde{M^0} = 0. \tag{4.9}$$

Let $\mathscr{I} = -\tau\mathcal{I}^\infty$. We have to solve

$$S^0 e^{\mathscr{I}} - \frac{\eta}{\tau}\mathscr{I} - \widetilde{M^0} = 0.$$

The solutions are given in terms of Lambert W function that is the multivalued inverse relation of the function $f(w) = we^w$ for $w \in \mathbb{C}$ [7]. Let us recall how to compute the real solutions of the equation $\alpha e^x + \beta x + \gamma = 0$ for $(\alpha, \beta, \gamma) \in \mathbb{R}^* \times \mathbb{R}^* \times \mathbb{R}$. Let $\Delta = \alpha/\beta \exp(-\gamma/\beta)$ be the discriminant. If $\Delta \geq 0$ or $\Delta = -\exp(-1)$, the solution is unique and $x = -W_0(\Delta) - \gamma/\beta$ where W_0 is the principal branch. If $\Delta \in (-\exp(-1), 0)$, there are two solutions $x_0 = -W_0(\Delta) - \gamma/\beta$ and $x_{-1} = -W_{-1}(\Delta) - \gamma/\beta$, where W_{-1} is another branch. When $\Delta < -\exp(-1)$, there is no solution.

In our symmetric case, the discriminant writes

$$\Delta = -\frac{S^0\tau}{\eta}\exp\left(-\frac{\widetilde{M^0}\tau}{\eta}\right).$$

Since $\Delta < 0$, there exist solutions to (4.9) if $\Delta \geq -\exp(-1)$, which is equivalent to

$$\exp\left(\frac{\widetilde{M^0}\tau}{\eta} - 1\right) \geq \frac{S^0\tau}{\eta}. \tag{4.10}$$

We recall that when we consider the standard SIR model (meaning in the context of this paper that we consider an isolated vertex), we can define the effective reproductive number $\mathscr{R}_e$ and the basic reproductive number $\mathscr{R}_0$ respectively given by

$$\mathscr{R}_e := \frac{S^0\tau}{\eta}, \quad \text{and} \quad \mathscr{R}_0 := \frac{M^0\tau}{\eta}, \tag{4.11}$$

see [10, 12, 26] for further properties of effective and basic reproductive numbers. If we denote $\widetilde{\mathscr{R}_0} = \widetilde{M^0}\tau/\eta$, the equation (4.10) reads

$$\exp\left(\widetilde{\mathscr{R}_0} - 1\right) \geq \mathscr{R}_e.$$

This inequality is satisfied as long as $S^0 \leq \widetilde{M^0}$, which is always true since $M^0 = \sum_{e\in\mathcal{E}} \int_{\Omega_e} u_e^0(x)\mathrm{d}x + c_{\mathcal{V}}\left(S^0 + I^0\right) \geq c_{\mathcal{V}} S^0$. Since $\Delta = -\mathscr{R}_e \exp(-\widetilde{\mathscr{R}_0})$, the solutions are

$$\mathscr{I}_{0,-1} = -W_{0,-1}\left(-\mathscr{R}_e \exp(-\widetilde{\mathscr{R}_0})\right) - \widetilde{\mathscr{R}_0},$$

and so

$$\mathcal{I}_{0,-1}^{\infty} = W_{0,-1}\left(-\mathscr{R}_e \exp(-\widetilde{\mathscr{R}_0})\right)/\tau + \widetilde{\mathscr{R}_0}/\tau.$$

Both $W_{0,-1}\left(-\mathscr{R}_e \exp(-\widetilde{\mathscr{R}_0})\right) < 0$. However, we can show that $\mathcal{I}_0^{\infty} > 0$ and $\mathcal{I}_{-1}^{\infty} < 0$. Thus, the only possibility is

$$\mathcal{I}^{\infty} = W_0\left(-\mathscr{R}_e \exp(-\widetilde{\mathscr{R}_0})\right)/\tau + \widetilde{\mathscr{R}_0}/\tau.$$

We also have access to S^{∞} and R^{∞} thanks to (4.4). Since $\exp(-W_0(x)) = W_0(x)/x$, we obtain

$$S^{\infty} = -\frac{\eta}{\tau} W_0\left(-\mathscr{R}_e \exp(-\widetilde{\mathscr{R}_0})\right),$$

and

$$R^{\infty} = \frac{\eta}{\tau} W_0\left(-\mathscr{R}_e \exp(-\widetilde{\mathscr{R}_0})\right) + \widetilde{M^0}.$$

We can summarize these results in the following lemma.

Lemma 4.3 (Fully symmetric case.)**.** *Assume that our model is fully symmetric, then the final total population of infected individuals as given by Theorem 2 is independent on the vertex that is $\mathcal{I}_v^{\infty} = \mathcal{I}^{\infty}$ for each $v \in \mathcal{V}$, and $\mathcal{I}^{\infty}$ has the following closed form formula*

$$\mathcal{I}^{\infty} = \frac{W_0\left(-\mathscr{R}_e \exp(-\mathscr{R}_0/c_{\mathcal{V}})\right)}{\tau} + \frac{\mathscr{R}_0}{c_{\mathcal{V}}\,\tau},$$

where $\mathscr{R}_e$ and $\mathscr{R}_0$ are respectively the effective and basic reproductive number defined in (4.11) and $c_{\mathcal{V}}$ the cardinal of $\mathcal{V}$. See Figure 3 for an illustration.

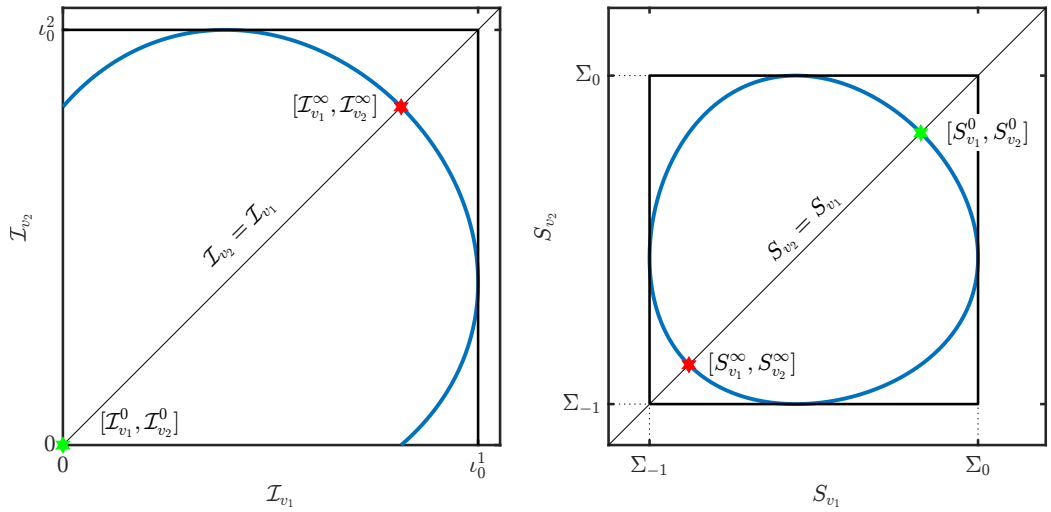

Figure 3: *Schematic visualisation (red star) of* $\mathcal{I}^\infty = \mathcal{I}_{v_1}^\infty = \mathcal{I}_{v_2}^\infty$*, resp.* $S^\infty = S_{v_1}^\infty = S_{v_2}^\infty$*, in the* $(\mathcal{I}_{v_1}, \mathcal{I}_{v_2})$ *plane, resp. in the* (S_{v_1}, S_{v_2})*-plane, in the fully symmetric case. The asymptotic value* $\mathcal{I}^\infty$*, resp.* S^∞*, lies at the intersection of the diagonal* $\mathcal{I}_{v_1} = \mathcal{I}_{v_2}$*, resp.* $S_{v_1} = S_{v_2}$*, and the implicit curve given by* (4.6)*, resp.* (4.7)*.*

Case of two vertices. In this simple case, it is possible to build explicit formulas to deal with the implicit submanifold equations (4.6), (4.7), and (4.8). Let $\mathscr{R}_{0,v_k} := M^0\,\tau_{v_k}/\eta_{v_k}$ and $\mathscr{R}_{e,v_k} := S_{v_k}^0\,\tau_{v_k}/\eta_{v_k}$, $k = 1, 2$ be respectively the local to vertex v_k basic and effective reproductive number. Then,

$$S_{v_1}^\infty = -\frac{\eta_{v_1}}{\tau_{v_1}} W\left(-\exp\left(-\mathscr{R}_{0,v_1}\right)\mathscr{R}_{e,v_1}\left(\mathscr{R}_{e,v_2}\right)^{\frac{\tau_{v_1}\eta_{v_2}}{\tau_{v_2}\eta_{v_1}}}\frac{\exp\left(S_{v_2}^\infty\,\tau_{v_1}/\eta_{v_1}\right)}{\left(S_{v_2}^\infty\,\tau_{v_2}/\eta_{v_2}\right)^{\frac{\tau_{v_1}\eta_{v_2}}{\tau_{v_2}\eta_{v_1}}}}\right), \tag{4.12}$$

where the Lambert W function W can be either W_0 or W_{-1}. Indeed, the argument of W being negative, two solutions have to be considered. We obviously also have

$$S_{v_2}^\infty = -\frac{\eta_{v_2}}{\tau_{v_2}} W\left(-\exp\left(-\mathscr{R}_{0,v_2}\right)\mathscr{R}_{e,v_2}\left(\mathscr{R}_{e,v_1}\right)^{\frac{\tau_{v_2}\eta_{v_1}}{\tau_{v_1}\eta_{v_2}}}\frac{\exp\left(S_{v_1}^\infty\,\tau_{v_2}/\eta_{v_2}\right)}{\left(S_{v_1}^\infty\,\tau_{v_1}/\eta_{v_1}\right)^{\frac{\tau_{v_2}\eta_{v_1}}{\tau_{v_1}\eta_{v_2}}}}\right), \tag{4.13}$$

Due to the definition of the domain of the Lambert W function, the argument has to be greater than $-\exp(-1)$. So, the following inequality must be satisfied for $S_{v_2}^\infty$ (respectively of $S_{v_1}^\infty$)

$$\frac{-\exp\left(-\mathscr{R}_{0,v_1}\right)\mathscr{R}_{e,v_1}\left(\mathscr{R}_{e,v_2}\right)^{\frac{\tau_{v_1}\eta_{v_2}}{\tau_{v_2}\eta_{v_1}}}}{\left(S_{v_2}^\infty\,\tau_{v_2}/\eta_{v_2}\right)^{\frac{\tau_{v_1}\eta_{v_2}}{\tau_{v_2}\eta_{v_1}}}\exp\left(-S_{v_2}^\infty\,\tau_{v_1}/\eta_{v_1}\right)} \geq -\exp(-1).$$

Solving the equality part of this inequality, we find that

$$S_{v_2}^\infty = -\frac{\eta_{v_2}}{\tau_{v_2}} W\left(-\left(\mathscr{R}_{e,v_1}\right)^{\frac{\tau_{v_2}\eta_{v_1}}{\tau_{v_1}\eta_{v_2}}}\mathscr{R}_{e,v_2}\exp\left(\frac{\tau_{v_2}\eta_{v_1}}{\tau_{v_1}\eta_{v_2}}\left(1-\mathscr{R}_{0,v_1}\right)\right)\right).$$

This equation has to be verified both for W_0 and W_{-1}. Let $\Sigma_{0,-1}^{v_2}$ be defined by

$$\Sigma_{0,-1}^{v_2} := -\frac{\eta_{v_2}}{\tau_{v_2}} W_{0,-1}\left(\mathscr{A}_{v_2}\right),$$

where

$$\mathscr{A}_{v_2} = (\mathscr{R}_{e,v_1})^{\frac{\tau_{v_2}\eta_{v_1}}{\tau_{v_1}\eta_{v_2}}} \mathscr{R}_{e,v_2} \exp\left(\frac{\tau_{v_2}\eta_{v_1}}{\tau_{v_1}\eta_{v_2}}\left(1-\mathscr{R}_{0,v_1}\right)\right) \tag{4.14}$$

Then, the domain of $S_{v_1}^{\infty}$ as a function of $S_{v_2}^{\infty}$ is

$$S_{v_2}^{\infty} \in \left[\min\left(\Sigma_{-1}^{v_2}, \Sigma_0^{v_2}\right), \max\left(\Sigma_{-1}^{v_2}, \Sigma_0^{v_2}\right)\right].$$

Concerning $S_{v_2}^{\infty}$ as a function of $S_{v_1}^{\infty}$, we have

$$S_{v_1}^{\infty} \in \left[\min\left(\Sigma_{-1}^{v_1}, \Sigma_0^{v_1}\right), \max\left(\Sigma_{-1}^{v_1}, \Sigma_0^{v_1}\right)\right],$$

with

$$\Sigma_{0,-1}^{v_1} := -\frac{\eta_{v_1}}{\tau_{v_1}} W_{0,-1}\left(\mathscr{A}_{v_1}\right),$$

where

$$\mathscr{A}_{v_1} = \mathscr{R}_{e,v_1} (\mathscr{R}_{e,v_2})^{\frac{\tau_{v_1}\eta_{v_2}}{\tau_{v_2}\eta_{v_1}}} \exp\left(\frac{\tau_{v_1}\eta_{v_2}}{\tau_{v_2}\eta_{v_1}}\left(1-\mathscr{R}_{0,v_2}\right)\right). \tag{4.15}$$

Thus,

$$\left(S_{v_1}^{\infty}, S_{v_2}^{\infty}\right) \in \Omega_S := \left[\min\left(\Sigma_{-1}^{v_1}, \Sigma_0^{v_1}\right), \max\left(\Sigma_{-1}^{v_1}, \Sigma_0^{v_1}\right)\right] \times \left[\min\left(\Sigma_{-1}^{v_2}, \Sigma_0^{v_2}\right), \max\left(\Sigma_{-1}^{v_2}, \Sigma_0^{v_2}\right)\right].$$

We present on Figure 4 (left) the functions W_0 and W_{-1} defining $S_{v_2}^{\infty}$ as a function of $S_{v_1}^{\infty}$ and the domain Ω_S for a given set of the parameters and initial conditions. We refer to Section 5 for details regarding the numerical integration of the model and Section 6 for further numerical results on the case of two vertices.

Actually, we can reduce the domain of validity of (4.12)-(4.13) for $S_{v_1}^{\infty}$ and $S_{v_2}^{\infty}$. Indeed, we know that S_{v_k}, $k = 1, 2$, decay with respect to time, so $S_{v_k}^{\infty} < S_{v_k}$. Moreover, the sum $S_{v_1}^{\infty} + S_{v_2}^{\infty} < M^0$. Thus, we have

$$\left(S_{v_1}^{\infty}, S_{v_2}^{\infty}\right) \in \omega_S := \left[\min\left(\Sigma_{-1}^{v_1}, \Sigma_0^{v_1}\right), S_{v_1}^0\right] \times \left[\min\left(\Sigma_{-1}^{v_2}, \Sigma_0^{v_2}\right), S_{v_2}^0\right] \cap \left\{S_{v_1}^{\infty} + S_{v_2}^{\infty} < M^0\right\}.$$

The domain ω_S is drawn on Figure 4 (right).

Concerning $\mathcal{I}_{v_1}^{\infty}$ and $\mathcal{I}_{v_2}^{\infty}$, we can perform the same analysis. Let

$$\mathcal{J}_{v_1}^{\infty} = -\mathscr{R}_{0,v_1} + \frac{\tau_{v_1}\eta_{v_2}}{\tau_{v_2}\eta_{v_1}}\left(\mathscr{R}_{e,v_2} \exp^{-\tau_{v_2}\mathcal{I}_{v_2}^{\infty}} + \tau_{v_2}\mathcal{I}_{v_2}^{\infty}\right),$$

and

$$\mathcal{J}_{v_2}^{\infty} = -\mathscr{R}_{0,v_2} + \frac{\tau_{v_2}\eta_{v_1}}{\tau_{v_1}\eta_{v_2}}\left(\mathscr{R}_{e,v_1} \exp^{-\tau_{v_1}\mathcal{I}_{v_1}^{\infty}} + \tau_{v_1}\mathcal{I}_{v_1}^{\infty}\right).$$

We obtain for $k = 1, 2$,

$$\mathcal{I}_{v_k}^{\infty} = \frac{1}{\tau_{v_k}} W\left(-\mathscr{R}_{e,v_k} \exp\left(\mathcal{J}_{v_k}^{\infty}\right)\right) - \frac{\mathcal{J}_{v_k}^{\infty}}{\tau_{v_k}},$$

still with W equal to W_{-1} and W_0. Let $\iota_{-1,0}^1$ and $\iota_{-1,0}^2$ be defined by

$$\iota_{-1,0}^{v_1} = \frac{W_{-1,0}\left(-\mathscr{A}_{v_1}\right)}{\tau_{v_1}} + \frac{\frac{\tau_{v_1}\eta_{v_2}}{\tau_{v_2}\eta_{v_1}}\left(\mathscr{R}_{0,v_2} - 1 - \log\left(\mathscr{R}_{e,v_2}\right)\right)}{\tau_{v_1}}, \tag{4.16}$$

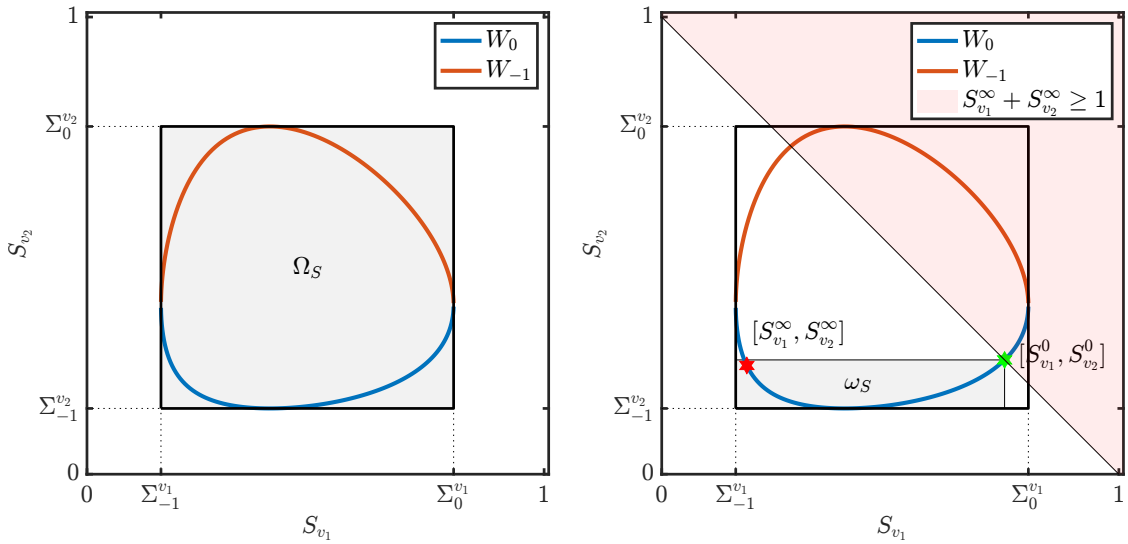

Figure 4: *Location of $S_{v_1}^\infty$ and $S_{v_2}^\infty$ together with the visualisation of the domains Ω_S (left) and ω_S (right). The final configuration of susceptible individuals $(S_{v_1}^\infty, S_{v_2}^\infty)$ lies on the closed curve parametrized by the two branches of the Lambert W function (blue and red curve). We note that $\left(S_{v_1}^\infty, S_{v_2}^\infty\right) \in \omega_S$ as indicated by the red star on the right figure. Values of the parameters are $d = 10^{-3}$, $\lambda^1 = \lambda^2 = 6/10$, $\alpha^1 = \alpha^2 = 1/8$, $\tau_{v_1} = 1$, $\tau_{v_2} = 9/10$, $\eta_{v_1} = 2/5$, $\eta_{v_2} = 2/6$, and initial conditions are set to: $I_1^0 = I_2^0 = 10^{-6}$, $S_0^1 = 3/4 - I_1^0$, $S_0^2 = 1/4 - I_1^0$ and $u^0(x) = 0$. The mass M^0 is therefore equal to 1.*

and

$$\iota_{-1,0}^{v_2} = \frac{W_{-1,0}\left(-\mathscr{A}_{v_2}\right)}{\tau_{v_2}} + \frac{\frac{\tau_{v_2}\eta_{v_1}}{\tau_{v_1}\eta_{v_2}}\left(\mathscr{R}_{0,v_1} - 1 - \log\left(\mathscr{R}_{e,v_1}\right)\right)}{\tau_{v_2}}, \tag{4.17}$$

with $\mathscr{A}_{v_1}$ and $\mathscr{A}_{v_2}$ given by (4.14) and (4.15). Then,

$$(\mathcal{I}_{v_1}^\infty, \mathcal{I}_{v_2}^\infty) \in [\min\left(\iota_{-1}^{v_1}, \iota_0^{v_1}\right), \max\left(\iota_{-1}^{v_1}, \iota_0^{v_1}\right)] \times [\min\left(\iota_{-1}^{v_2}, \iota_0^{v_2}\right), \max\left(\iota_{-1}^{v_2}, \iota_0^{v_2}\right)].$$

We can show that $\min\left(\iota_{-1}^{v_k}, \iota_0^{v_k}\right) < 0$ for $k = 1, 2$. So, we can reduce this domain since $\mathcal{I}_{v_k}^\infty > 0$. So, we define the domain $\omega_{\mathcal{I}}$

$$(\mathcal{I}_{v_1}^\infty, \mathcal{I}_{v_2}^\infty) \in \omega_{\mathcal{I}} := [0, \max\left(\iota_{-1}^{v_1}, \iota_0^{v_1}\right)] \times [0, \max\left(\iota_{-1}^{v_2}, \iota_0^{v_2}\right)].$$

As a consequence, we have proved the following lemma.

Lemma 4.4. *Case of two vertices. Assume that $|\mathcal{V}| = 2$ and $|\mathcal{E}| = 1$. The final total population of infected individuals at each vertex $\mathcal{I}_{v_k}^\infty$, $k = 1, 2$ can be expressed as*

$$\mathcal{I}_{v_k}^\infty = \frac{1}{\tau_{v_k}} W\left(-\mathscr{R}_{e,v_k} \exp\left(\mathcal{J}_{v_k}^\infty\right)\right) - \frac{\mathcal{J}_{v_k}^\infty}{\tau_{v_k}},$$

with

$$\mathcal{J}_{v_k}^\infty = -\mathscr{R}_{0,v_k} + \frac{\tau_{v_k}\eta_{v_j}}{\tau_{v_j}\eta_{v_k}}\left(\mathscr{R}_{e,v_j} \exp^{-\tau_{v_j}\mathcal{I}_{v_j}^\infty} + \tau_{v_j}\mathcal{I}_{v_j}^\infty\right), \quad k \neq j \in \{1, 2\},$$

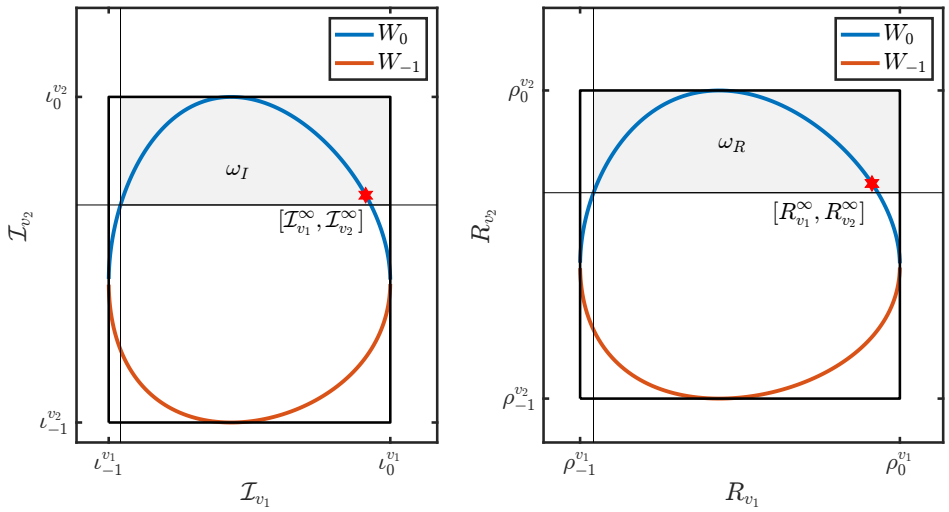

Figure 5: *Location of $\mathcal{I}_k^\infty$ and $R_{v_k}^\infty$, $k = 1, 2$, and visualisation of the domains $\omega_\mathcal{I}$ (left), and domain ω_R (right). In both cases, $(\mathcal{I}_1^\infty, \mathcal{I}_2^\infty) \in \omega_\mathcal{I}$ and $(R_1^\infty, R_2^\infty) \in \omega_R$ are represented by a red star. Values of the parameters and initial conditions are similar to Figure 4.*

where $\mathscr{R}_{0,v_k} := M^0\, \tau_{v_k}/\eta_{v_k}$ and $\mathscr{R}_{e,v_k} := S_{v_k}^0\, \tau_{v_k}/\eta_{v_k}$, $k = 1, 2$. Furthermore, we have the sharp bound

$$(\mathcal{I}_{v_1}^\infty, \mathcal{I}_{v_2}^\infty) \in \omega_\mathcal{I} := [0, \max\left(\iota_{-1}^{v_1}, \iota_0^{v_1}\right)] \times [0, \max\left(\iota_{-1}^{v_2}, \iota_0^{v_2}\right)],$$

with $\iota_{-1,0}^{v_k}$, $k = 1, 2$ defined in (4.16)-(4.17). See Figure 5 for an illustration.

Remark 4.5. *As the solutions $R_{v_k}^\infty$, $k = 1, 2$, are simply given by $R_{v_k}^\infty = \eta_{v_k} \mathcal{I}_{v_k}^\infty$, if we let $\rho_{-1,0}^{v_k} := \eta \iota_{-1,0}^{v_k}$ then we have*

$$(R_{v_1}^\infty, R_{v_2}^\infty) \in \omega_R := [0, \max\left(\rho_{-1}^{v_1}, \rho_0^{v_1}\right)] \times [0, \max\left(\rho_{-1}^{v_2}, \rho_0^{v_2}\right)].$$

We represent on Figure 5 the domain ω_R.

5 A semi-implicit numerical scheme which preserves total mass

In this section, we propose a semi-implicit in time numerical scheme based on finite differences in space which has the property to preserve the *discrete* total mass.

5.1 Notations

For each $e \in \mathcal{E}$, we denote $\delta x_e > 0$ the space discretization of each edge, and $J_e \in \mathbb{N}$ the number of points of the corresponding discretization. For each $i = 1, \cdots, J_e$, the space grid on each edge is given by $x_i = (i-1)\delta x_e$ with $\ell_e = (J_e - 1)\delta x_e$. And we let $\mathbf{J} := \sum_{e \in \mathcal{E}} J_e \in \mathbb{N}$. Let $\delta t > 0$ be the time discretization and denote $t_m = m\delta t$ for $m \geq 0$.

For a given function $u \in \mathscr{C}^{1,2}(\mathbb{R}_+ \times \mathcal{G}, \mathbb{R}^+)$, its space-time discretization is given by some sequence of vectors

$$u \sim (U^m)_{m\geq 0}, \text{ with } U^m = (U_1^m, \cdots, U_{\mathbf{J}}^m)^{\mathbf{t}} \in \mathbb{R}^{\mathbf{J}}.$$

For each $e \in \mathcal{E}$, there exists an integer $j_e \in \mathbb{N}$ such that

$$u_e(t_m, x_i) \sim U_{j_e+i}^m, \quad i = 1, \cdots, J_e, \quad m \geq 0.$$

We approximate the laplacian on each edge via finite differences. That is, for each $e \in \mathcal{E}$,

$$\partial_x^2 u_e(t_m, x_i) \sim \frac{U_{j_e+i-1}^m - 2U_{j_e+i}^m + U_{j_e+i+1}^m}{\delta x_e^2}, \quad i = 2, \cdots, J_e - 1, \quad m \geq 1,$$

where we have only considered the interior points of the discretized domain. Let us now precise how we approximate the laplacian at a given vertex $v \in \mathcal{V}$ of the graph. So let $v \in \mathcal{V}$ such that there are δ_v edges incident to the vertex. We locally label $e \sim v = (e_1, \cdots, e_{\delta_v})$ all these incident edges. For each $v \in \mathcal{V}$, we introduce the map $\sigma_v : \{e_1, \cdots, e_{\delta_v}\} \to \{1, \cdots, \mathbf{J}\}$ such that $\sigma_v(e_k)$ corresponds to the global index of the grid discretization associated to the vertex v on edge e_k. Finally, we denote by $n(\sigma_v(e_k))$ the global index of the nearest neighbor on edge e_k to the vertex v. Note that either $n(\sigma_v(e_k)) = \sigma_v(e_k) - 1$ or $n(\sigma_v(e_k)) = \sigma_v(e_k) + 1$. To approximate the laplacian at a given vertex $v \in \mathcal{V}$ on edge e_k, we use the following formula

$$\partial_x^2 u_{e_k}(t_m, v) \sim \frac{U_{\sigma_v(e_k)}^{*,m} - 2U_{\sigma_v(e_k)}^m + U_{n(\sigma_v(e_k))}^m}{\delta x_{e_k}^2} := \mathcal{Z}_{v,k}^m, \quad k = 1, \cdots, \delta_v, \quad m \geq 1.$$

The unknown $U_{\sigma_v(e_k)}^{*,m}$ can be expressed by discretization of the boundary condition as follows. For each $v \in \mathcal{V}$ with $e \sim v = (e_1, \cdots, e_{\delta_v})$, we approximate the normal derivative $\partial_n u_{e_k}(t_m, v)$ as

$$\partial_n u_{e_k}(t_m, v) \sim \frac{U_{\sigma_v(e_k)}^{*,m} - U_{n(\sigma_v(e_k))}^m}{2\delta x_{e_k}}, \quad k = 1, \cdots, \delta_v, \quad m \geq 1.$$

Using (2.3), and denoting I_v^m the time approximation of $I_v(t_m)$, we obtain the following expression for $U_{\sigma_v(e_k)}^{*,m}$

$$U_{\sigma_v(e_k)}^{*,m} = U_{n(\sigma_v(e_k))}^m - \frac{2\delta x_{e_k}}{d_{e_k}} \left(\alpha_{e_k}^v U_{\sigma_v(e_k)}^m + \sum_{l=1}^{\delta_v} (N_v)_{kl} U_{\sigma_v(e_l)}^m - \lambda_{e_k}^v I_v^m \right), \quad k = 1, \cdots, \delta_v, \quad m \geq 1.$$

As a consequence, we obtain that for each $k = 1, \cdots, \delta_v$ and $m \geq 1$

$$\mathcal{Z}_{v,k}^m = \frac{2U_{n(\sigma_v(e_k))}^m - 2U_{\sigma_v(e_k)}^m}{\delta x_{e_k}^2} - \frac{2}{d_{e_k}\delta x_{e_k}} \left(\alpha_{e_k}^v U_{\sigma_v(e_k)}^m + \sum_{l=1}^{\delta_v} (N_v)_{kl} U_{\sigma_v(e_l)}^m - \lambda_{e_k}^v I_v^m \right).$$

5.2 The semi-implicit numerical scheme

We introduce the following scheme for each $m \geq 0$

$$\begin{cases} U_{j_e+i}^{m+1} = U_{j_e+i}^{m} + d_e \delta t \left(\dfrac{U_{j_e+i-1}^{m+1} - 2U_{j_e+i}^{m+1} + U_{j_e+i+1}^{m+1}}{\delta x_e^2} \right), \quad i = 2, \cdots, J_e - 1, \quad e \in \mathcal{E}, \\ U_{\sigma_v(e_k)}^{m+1} = U_{\sigma_v(e_k)}^{m} + d_{e_k} \delta t \mathcal{Z}_{v,k}^{m+1}, \quad k = 1, \cdots, \delta_v, \quad v \in \mathcal{V}, \\ S_v^{m+1} = S_v^m - \delta t \tau_v S_v^{m+1} I_v^m, \\ I_v^{m+1} = I_v^m + \delta t \left(\tau_v S_v^{m+1} I_v^m - \eta_v I_v^{m+1} \right) + \delta t \left(\displaystyle\sum_{k=1}^{\delta_v} \alpha_{e_k}^v U_{\sigma_v(e_k)}^{m+1} - \overline{\lambda}_v I_v^{m+1} \right), \\ R_v^{m+1} = R_v^m + \delta t \eta_v I_v^{m+1}, \end{cases} \tag{5.1}$$

initialized with $U^0 \in \mathbb{R}^{\mathbf{J}}$ and some $(S_v^0, I_v^0, R_v^0)_{v \in \mathcal{V}}$. One can find similar semi-implicit discretization for the SIR part of the model in [23].

Well-posedness and positivity. We prove that the numerical scheme defined through (5.1) is well defined and preserves positivity under some condition on δt. Indeed, we first remark that the equation for S_v^{m+1} and I_v^{m+1} in (5.1) can be used to obtain that

$$\begin{aligned} S_v^{m+1} &= \frac{S_v^m}{1 + \delta t \tau_v I_v^m}, \\ I_v^{m+1} &= \frac{I_v^m + \delta t \tau_v I_v^m (S_v^m + I_v^m)}{\left(1 + \delta t (\eta_v + \overline{\lambda}_v)\right)\left(1 + \delta t \tau_v I_v^m\right)} + \frac{\delta t}{1 + \delta t (\eta_v + \overline{\lambda}_v)} \sum_{l=1}^{\delta_v} \alpha_{e_l}^v U_{\sigma_v(e_l)}^{m+1}, \end{aligned}$$

such that $\mathcal{Z}_{v,k}^{m+1}$ can be expressed only in terms of elements of U^{m+1} as

$$\begin{aligned} \mathcal{Z}_{v,k}^{m+1} = &\frac{2U_{n(\sigma_v(e_k))}^{m+1} - 2U_{\sigma_v(e_k)}^{m+1}}{\delta x_{e_k}^2} - \frac{2}{d_{e_k} \delta x_{e_k}} \left(\alpha_{e_k}^v U_{\sigma_v(e_k)}^{m+1} + \sum_{l=1}^{\delta_v} (N_v)_{kl} U_{\sigma_v(e_l)}^{m+1} - \frac{\delta t \lambda_{e_k}^v}{1 + \delta t (\eta_v + \overline{\lambda}_v)} \sum_{l=1}^{\delta_v} \alpha_{e_l}^v U_{\sigma_v(e_l)}^{m+1} \right) \\ &+ \frac{2\lambda_{e_k}^v}{d_{e_k} \delta x_{e_k}} \left(\frac{I_v^m + \delta t \tau_v I_v^m (S_v^m + I_v^m)}{\left(1 + \delta t (\eta_v + \overline{\lambda}_v)\right)\left(1 + \delta t \tau_v I_v^m\right)} \right). \end{aligned}$$

As a consequence, there exists a matrix $\mathcal{A} \in \mathscr{M}_{\mathbf{J}}(\mathbb{R})$ such that

$$\left(\mathrm{I}_{\mathbf{J}} + \mathcal{A}\right) U^{m+1} = U^m + \mathcal{Y}^m,$$

where $\mathcal{Y}^m \in \mathbb{R}^{\mathbf{J}}$ is such that

$$\mathcal{Y}_j^m = \begin{cases} \dfrac{2\delta t \lambda_{e_k}^v}{\delta x_{e_k}} \left(\dfrac{I_v^m + \delta t \tau_v I_v^m (S_v^m + I_v^m)}{\left(1 + \delta t (\eta_v + \overline{\lambda}_v)\right)\left(1 + \delta t \tau_v I_v^m\right)} \right) & , \text{ if } j = \sigma_v(e_k), \\ 0 & , \text{ otherwise.} \end{cases}$$

Lemma 5.1. *There exists a constant $C_0 > 0$, which only depends on the parameters of the system, such that if $0 < \delta t < C_0$ then we have*

- $\mathrm{I}_{\mathbf{J}} + \mathcal{A}$ *is invertible;*
- *if* N_v *is symmetric for each* $v \in \mathcal{V}$*, then given* $V \in \mathbb{R}^{\mathbf{J}}$ *with* $V \geq \mathbf{0}$*, the unique solution* $U \in \mathbb{R}^{\mathbf{J}}$ *of* $(\mathrm{I}_{\mathbf{J}} + \mathcal{A})U = V$ *also satisfies* $U \geq \mathbf{0}$*.*

Proof. Let $U \in \mathbb{R}^{\mathbf{J}} \neq \mathbf{0}$ be such that $(\mathrm{I}_{\mathbf{J}} + \mathcal{A})U = 0$. Without loss of generality, assume that $U_{j_0} = \max_{j=1,\cdots,\mathbf{J}} U_j > 0$. If there exists $e \in \mathcal{E}$ such that $j_0 = j_e + i_0$ for some $i_0 \in \{2, \cdots, J_e - 1\}$, then we have

$$U_{j_0} + \frac{d_e \delta t}{\delta x_e^2}(2U_{j_0} - U_{j_0-1} - U_{j_0+1}) = 0,$$

which is a contradiction by definition of U_{j_0}. Next if j_0 is such that there is $v \in \mathcal{V}$ and $k \in \{1, \cdots, \delta_v\}$ such that $j_0 = \sigma_v(e_k)$, then we have

$$U_{\sigma_v(e_k)} + \frac{2d_{e_k}\delta t}{\delta x_{e_k}^2}(U_{\sigma_v(e_k)} - U_{n(\sigma_v(e_k))}) = -\frac{2\delta t}{\delta x_{e_k}}\left(\alpha_{e_k}^v U_{\sigma_v(e_k)} + \sum_{l=1}^{\delta_v}(N_v)_{kl}U_{\sigma_v(e_l)} - \frac{\delta t \lambda_{e_k}^v}{1 + \delta t(\eta_v + \overline{\lambda}_v)}\sum_{l=1}^{\delta_v}\alpha_{e_l}^v U_{\sigma_v(e_l)}\right).$$

The left-hand side of the above equality is strictly positive and we claim that the right-hand side is negative. We use the fact that $(N_v)_{kl} = -\nu_{e_l,e_k}^v$ when $k \neq l$ and $(N_v)_{kk} = \sum_{j\neq k}\nu_{e_k,e_j}^v$

$$\begin{aligned}\sum_{l=1}^{\delta_v}(N_v)_{kl}U_{\sigma_v(e_l)} &= \left(\sum_{j\neq k}\nu_{e_k,e_j}^v\right)U_{\sigma_v(e_k)} - \sum_{l\neq k}\nu_{e_l,e_k}^v U_{\sigma_v(e_l)} \\ &= \left[\sum_{j\neq k}\nu_{e_k,e_j}^v - \sum_{l\neq k}\nu_{e_l,e_k}^v\right]U_{\sigma_v(e_k)} + \sum_{l\neq k}\nu_{e_l,e_k}^v\left(U_{\sigma_v(e_k)} - U_{\sigma_v(e_l)}\right).\end{aligned}$$

As a consequence, we deduce that

$$\begin{aligned}\mathcal{U}_k^v &:= \alpha_{e_k}^v U_{\sigma_v(e_k)} + \sum_{l=1}^{\delta_v}(N_v)_{kl}U_{\sigma_v(e_l)} - \frac{\delta t\lambda_{e_k}^v}{1+\delta t(\eta_v+\overline{\lambda}_v)}\sum_{l=1}^{\delta_v}\alpha_{e_l}^v U_{\sigma_v(e_l)} \\ &= \left[\alpha_{e_k}^v + \sum_{j\neq k}\nu_{e_k,e_j}^v - \sum_{l\neq k}\nu_{e_l,e_k}^v - \frac{\delta t\lambda_{e_k}^v}{1+\delta t(\eta_v+\overline{\lambda}_v)}\sum_{l=1}^{\delta_v}\alpha_{e_l}^v\right]U_{\sigma_v(e_k)} + \sum_{l\neq k}\nu_{e_l,e_k}^v\left(U_{\sigma_v(e_k)} - U_{\sigma_v(e_l)}\right) \\ &\quad + \frac{\delta t\lambda_{e_k}^v}{1+\delta t(\eta_v+\overline{\lambda}_v)}\sum_{l=1}^{\delta_v}\alpha_{e_l}^v\left(U_{\sigma_v(e_k)} - U_{\sigma_v(e_l)}\right).\end{aligned}$$

The last two terms are positive by definition of $U_{j_0} = U_{\sigma_v(e_k)} = \max_{j=1,\cdots,\mathbf{J}} U_j > 0$. Now using Hypothesis 2.2, we have that

$$\alpha_{e_k}^v + \sum_{j\neq k}\nu_{e_k,e_j}^v - \sum_{l\neq k}\nu_{e_l,e_k}^v > 0,$$

such that the term in bracket is positive provided that

$$\frac{\delta t\lambda_{e_k}^v}{1+\delta t(\eta_v+\overline{\lambda}_v)}\sum_{l=1}^{\delta_v}\alpha_{e_l}^v < \alpha_{e_k}^v + \sum_{j\neq k}\nu_{e_k,e_j}^v - \sum_{l\neq k}\nu_{e_l,e_k}^v,$$

or equivalently

$$\delta t\left[\lambda_{e_k}^v\sum_{l=1}^{\delta_v}\alpha_{e_l}^v-(\eta_v+\overline{\lambda}_v)\left(\alpha_{e_k}^v+\sum_{j\neq k}\nu_{e_k,e_j}^v-\sum_{l\neq k}\nu_{e_l,e_k}^v\right)\right]<\alpha_{e_k}^v+\sum_{j\neq k}\nu_{e_k,e_j}^v-\sum_{l\neq k}\nu_{e_l,e_k}^v.$$

As a consequence, we impose that

$$0<\delta t<\min_{v\in\mathcal{V}}\min_{k=1,\cdots,\delta_v}\frac{\alpha_{e_k}^v+\sum_{j\neq k}\nu_{e_k,e_j}^v-\sum_{l\neq k}\nu_{e_l,e_k}^v}{\left[\lambda_{e_k}^v\sum_{l=1}^{\delta_v}\alpha_{e_l}^v-(\eta_v+\overline{\lambda}_v)\left(\alpha_{e_k}^v+\sum_{j\neq k}\nu_{e_k,e_j}^v-\sum_{l\neq k}\nu_{e_l,e_k}^v\right)\right]_+},$$

where it is understood that when the positive part is zero there is no condition on δt. And we have reached a contradiction since

$$0<U_{\sigma_v(e_k)}+\frac{2d_{e_k}\delta t}{\delta x_{e_k}^2}(U_{\sigma_v(e_k)}-U_{n(\sigma_v(e_k))})=-\frac{2\delta t}{\delta x_{e_k}}\mathcal{U}_k^v<0.$$

This shows that $\mathrm{I}_{\mathbf{J}}+\mathcal{A}$ is invertible.

Next let $U\in\mathbb{R}^{\mathbf{J}}$ be the unique solution of $(\mathrm{I}_{\mathbf{J}}+\mathcal{A})U=V$ with $V\geq\mathbf{0}$. We denote by $U^-\in\mathbb{R}^{\mathbf{J}}$ the vector with components given by

$$U_j^-=\min(0,U_j),\quad j=1,\cdots,\mathbf{J}.$$

Our aim is to evaluate $\langle(\mathrm{I}_{\mathbf{J}}+\mathcal{A})U,U^-\rangle_{\mathbf{J}}$ where $\langle\cdot,\cdot\rangle_{\mathbf{J}}$ is the following scalar product on $\mathbb{R}^{\mathbf{J}}$:

$$\langle U,V\rangle_{\mathbf{J}}:=\sum_{e\in\mathcal{E}}\left(\sum_{i=2}^{J_e-1}U_{j_e+i}V_{j_e+i}\right)+\frac{1}{2}\sum_{v\in\mathcal{V}}\left(\sum_{k=1}^{\delta_v}U_{\sigma_v(e_k)}V_{\sigma_v(e_k)}\right).$$

We divide $\langle(\mathrm{I}_{\mathbf{J}}+\mathcal{A})U,U^-\rangle_{\mathbf{J}}$ into three parts:

$$\langle(\mathrm{I}_{\mathbf{J}}+\mathcal{A})U,U^-\rangle_{\mathbf{J}}=\mathcal{Q}_1+\mathcal{Q}_2+\mathcal{Q}_3,$$

where

$$\begin{aligned}
\mathcal{Q}_1&:=\sum_{e\in\mathcal{E}}\sum_{i=2}^{J_e-1}\left(U_{j_e+i}+\frac{d_e\delta t}{\delta x_e^2}\left(2U_{j_e+i}-U_{j_e+i-1}-U_{j_e+i+1}\right)\right)U_{j_e+i}^-,\\
\mathcal{Q}_2&:=\frac{1}{2}\sum_{v\in\mathcal{V}}\sum_{k=1}^{\delta_v}\left(U_{\sigma_v(e_k)}+\frac{2d_{e_k}\delta t}{\delta x_{e_k}^2}\left(U_{\sigma_v(e_k)}-U_{n(\sigma_v(e_k))}\right)\right)U_{\sigma_v(e_k)}^-,\\
\mathcal{Q}_3&:=\delta t\sum_{v\in\mathcal{V}}\sum_{k=1}^{\delta_v}\frac{1}{\delta x_{e_k}}\left(\alpha_{e_k}^vU_{\sigma_v(e_k)}+\sum_{l=1}^{\delta_v}(N_v)_{kl}U_{\sigma_v(e_l)}-\frac{\delta t\lambda_{e_k}^v}{1+\delta t(\eta_v+\overline{\lambda}_v)}\sum_{l=1}^{\delta_v}\alpha_{e_l}^vU_{\sigma_v(e_l)}\right)U_{\sigma_v(e_k)}^-.
\end{aligned}$$

The first and second terms are handled as follows

$$\mathcal{Q}_1+\mathcal{Q}_2=\langle U,U^-\rangle_{\mathbf{J}}+\sum_{e\in\mathcal{E}}\frac{d_e\delta t}{\delta x_e^2}\sum_{i=1}^{J_e-1}\left(U_{j_e+i+1}-U_{j_e+i}\right)\left(U_{j_e+i+1}^--U_{j_e+i}^-\right)\geq 0.$$

For the third term $\mathcal{Q}_3$, if we further assume that N_v is symmetric, then the matrix $K_v = A_v + N_v$ is symmetric positive definite, and thus for each $v \in \mathcal{V}$ there exists some $\beta_v > 0$ such that

$$\sum_{k=1}^{\delta_v} \frac{1}{\delta x_{e_k}} \left(\alpha_{e_k}^v U_{\sigma_v(e_k)} + \sum_{l=1}^{\delta_v} (N_v)_{kl} U_{\sigma_v(e_l)} \right) U^-_{\sigma_v(e_k)} \geq \beta_v \sum_{k=1}^{\delta_v} \frac{1}{\delta x_{e_k}} U_{\sigma_v(e_k)} U^-_{\sigma_v(e_k)},$$

while there exists $\omega_v > 0$ such that

$$\left(\sum_{k=1}^{\delta_v} \frac{\lambda_{e_k}}{\delta x_{e_k}} U^-_{\sigma_v(e_k)} \right) \left(\sum_{l=1}^{\delta_v} \alpha_{e_l}^v U_{\sigma_v(e_l)} \right) \leq \omega_v \sum_{k=1}^{\delta_v} \frac{1}{\delta x_{e_k}} U_{\sigma_v(e_k)} U^-_{\sigma_v(e_k)}.$$

And thus, we get an estimate for $\mathcal{Q}_3$ of the form

$$\mathcal{Q}_3 \geq \delta t \sum_{v \in \mathcal{V}} \left[\left(\beta_v - \frac{\delta t \omega_v}{1 + \delta t(\eta_v + \overline{\lambda}_v)} \right) \sum_{k=1}^{\delta_v} \frac{1}{\delta x_{e_k}} U_{\sigma_v(e_k)} U^-_{\sigma_v(e_k)} \right],$$

which is positive provided that δt is small enough. As a consequence, we have proved that

$$0 \leq \langle (\mathrm{I}_{\mathbf{J}} + \mathcal{A}) U, U^- \rangle_{\mathbf{J}} = \langle V, U^- \rangle_{\mathbf{J}} \leq 0,$$

which implies that $U^- = \mathbf{0}$ and thus $U \geq \mathbf{0}$. ∎

The previous lemma demonstrates the well-posedness of our numerical scheme (5.1). It also ensures that if we start with positive initial conditions $U^0 \geq \mathbf{0}$ and $S_v^0 > 0$, $I_v^0 \geq 0$ with $\sum_{v \in \mathcal{V}} I_v^0 > 0$ and $R_v^0 \geq 0$, then for all $m \geq 1$ we also have that $U^m \geq \mathbf{0}$, $S_v^m > 0$, $I_v^m \geq 0$ and $R_v^m \geq 0$, provided $\delta t > 0$ is small enough and N_v is symmetric for each $v \in \mathcal{V}$.

Preservation of total discrete mass. For any $U \in \mathbb{R}^{\mathbf{J}}$, we define the following quantity

$$\mathrm{trap}_{\mathbf{J}}(U) := \sum_{e \in \mathcal{E}} \delta x_e \left(\sum_{i=2}^{J_e - 1} U_{j_e + i} \right) + \frac{1}{2} \sum_{v \in \mathcal{V}} \delta x_{e_k} \left(\sum_{k=1}^{\delta_v} U_{\sigma_v(e_k)} \right).$$

The expression $\mathrm{trap}_{\mathbf{J}}(U)$ is simply the trapezoidal rule applied to the elements of U adapted to our graph $\mathcal{G}$. From (5.1), we get that

$$\begin{aligned} \mathrm{trap}_{\mathbf{J}}(U^{m+1}) = \mathrm{trap}_{\mathbf{J}}(U^m) &+ \delta t \sum_{e \in \mathcal{E}} \frac{d_e}{\delta x_e} \left(\sum_{i=2}^{J_e - 1} \left(U_{j_e+i-1}^{m+1} - 2U_{j_e+i}^{m+1} + U_{j_e+i+1}^{m+1} \right) \right) \\ &+ \frac{\delta t}{2} \sum_{v \in \mathcal{V}} \delta x_{e_k} d_{e_k} \left(\sum_{k=1}^{\delta_v} \mathcal{Z}_{v,k}^{m+1} \right). \end{aligned}$$

Upon denoting $\mathcal{Z}_{v,k}^{1,m}$ the following quantity

$$\mathcal{Z}_{v,k}^{1,m} := \frac{2U_{n(\sigma_v(e_k))}^m - 2U_{\sigma_v(e_k)}^m}{\delta x_{e_k}^2}$$

we get that

$$\frac{1}{2}\sum_{v\in\mathcal{V}}\delta x_{e_k}d_{e_k}\left(\sum_{k=1}^{\delta_v}\mathcal{Z}_{v,k}^{1,m+1}\right)=\sum_{v\in\mathcal{V}}\frac{d_{e_k}}{\delta x_{e_k}}\left(\sum_{k=1}^{\delta_v}U_{n(\sigma_v(e_k))}^{m+1}-U_{\sigma_v(e_k)}^{m+1}\right).$$

Next, we observe that

$$\sum_{e\in\mathcal{E}}\frac{d_e}{\delta x_e}\left(\sum_{i=2}^{J_e-1}\left(U_{j_e+i-1}^{m+1}-2U_{j_e+i}^{m+1}+U_{j_e+i+1}^{m+1}\right)\right)+\sum_{v\in\mathcal{V}}\frac{d_{e_k}}{\delta x_{e_k}}\left(\sum_{k=1}^{\delta_v}U_{n(\sigma_v(e_k))}^{m+1}-U_{\sigma_v(e_k)}^{m+1}\right)=0,$$

where the cancellation comes from the specific structure of the discretized laplacian through finite differences. As a consequence, we have that

$$\mathrm{trap}_{\mathbf{J}}(U^{m+1})=\mathrm{trap}_{\mathbf{J}}(U^m)-\delta t\sum_{v\in\mathcal{V}}\sum_{k=1}^{\delta_v}\left(\alpha_{e_k}^v U_{\sigma_v(e_k)}^{m+1}+\sum_{l=1}^{\delta_v}(N_v)_{kl}U_{\sigma_v(e_l)}^{m+1}-\lambda_{e_k}^v I_v^{m+1}\right).$$

We also have that

$$\sum_{k=1}^{\delta_v}\sum_{l=1}^{\delta_v}(N_v)_{kl}U_{\sigma_v(e_l)}^{m+1}=\sum_{l=1}^{\delta_v}\left(\sum_{k=1}^{\delta_v}(N_v)_{kl}\right)U_{\sigma_v(e_l)}^{m+1}=0,$$

as the sum over the lines of N_v vanishes. And thus we get

$$\mathrm{trap}_{\mathbf{J}}(U^{m+1})=\mathrm{trap}_{\mathbf{J}}(U^m)-\delta t\sum_{v\in\mathcal{V}}\left(\sum_{k=1}^{\delta_v}\alpha_{e_k}^v U_{\sigma_v(e_k)}^{m+1}-\overline{\lambda}_v I_v^{m+1}\right).$$

On the other hand, from (5.1) we also have

$$\sum_{v\in\mathcal{V}}\left(S_v^{m+1}+I_v^{m+1}+R_v^{m+1}\right)=\sum_{v\in\mathcal{V}}\left(S_v^m+I_v^m+R_v^m\right)+\delta t\sum_{v\in\mathcal{V}}\left(\sum_{k=1}^{\delta_v}\alpha_{e_k}^v U_{\sigma_v(e_k)}^{m+1}-\overline{\lambda}_v I_v^{m+1}\right).$$

As a conclusion, we have proved the following result.

Lemma 5.2. *Let (U^m,S_v^m,I_v^m,R_v^m) a solution of (5.1), then we have for each $m\geq 0$*

$$\mathrm{trap}_{\mathbf{J}}(U^{m+1})+\sum_{v\in\mathcal{V}}\left(S_v^{m+1}+I_v^{m+1}+R_v^{m+1}\right)=\mathrm{trap}_{\mathbf{J}}(U^m)+\sum_{v\in\mathcal{V}}\left(S_v^m+I_v^m+R_v^m\right).$$

This is the discrete conter part of conservation of mass for the continuous model.

Now, combining Lemma 5.1-5.2, we have proved the following theorem.

Theorem 3. *There exists a constant $C_0>0$, which only depends on the parameters of the system, such that if $0<\delta t<C_0$, then the numerical scheme (5.1) defines a unique sequence $(U^m,S_v^m,I_v^m,R_v^m)_{m\geq 0}$. If we further assume that N_v is symmetric for each $v\in\mathcal{V}$, then the numerical scheme (5.1) preserves the positivity of the initial condition. Finally, for each solution of (5.1), the total discrete mass is preserved, namely for each $m\geq 0$, we have*

$$\mathrm{trap}_{\mathbf{J}}(U^{m+1})+\sum_{v\in\mathcal{V}}\left(S_v^{m+1}+I_v^{m+1}+R_v^{m+1}\right)=\mathrm{trap}_{\mathbf{J}}(U^m)+\sum_{v\in\mathcal{V}}\left(S_v^m+I_v^m+R_v^m\right).$$

6 Numerical results for a selection of graphs

In the present section, we illustrate our theoretical results with a collection of numerical simulations for various types of graphs. Throughout this section the time discretization is set to $\delta t = 0.01$ while the space discretization to $\delta_{x_e} = 0.01$ for each $e \in \mathcal{E}$.

6.1 Case of 2 vertices and 1 edge

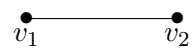

We first consider the case where $c_{\mathcal{V}} = 2$ and $c_{\mathcal{E}} = 1$, where $c_{\mathcal{E}}$ denotes the cardinal of $\mathcal{E}$. In this setting, we recall that our model reads as follows

$$\partial_t u(t,x) = d\partial_x^2 u(t,x), \quad t > 0, \quad x \in (0,\ell),$$

with boundary conditions

$$\begin{cases} -d\partial_x u(t,0) + \alpha_1 u(t,0) = \lambda_1 I_1(t), \\ \quad d\partial_x u(t,\ell) + \alpha_2 u(t,\ell) = \lambda_2 I_2(t), \end{cases} \quad t > 0,$$

where $(S_i(t), I_i(t), R_i(t))$, for $i = 1, 2$, solution of

$$\begin{cases} S_i'(t) = -\tau_i S_i(t) I_i(t), \\ I_i'(t) = \tau_i S_i(t) I_i(t) - \eta_i I_v(t) + \alpha_i u(t, v_i) - \lambda_i I_i(t), \quad t > 0, \\ R_i'(t) = \eta_i I_i(t), \end{cases}$$

where $v_1 = 0$ and $v_2 = \ell$. This system is complemented by some initial condition $(u^0, S_i^0, I_i^0, R_i^0)$ with $S_i > 0$, $I_1^0 + I_2^0 > 0$, $R_i^0 = 0$ and $u^0 \geq 0$ such that the boundary condition is satisfied initially. Finally, we normalize the total mass as follows

$$M^0 = \int_0^\ell u^0(x)\mathrm{d}x + \sum_{i=1}^{2} \left(S_i^0 + I_i^0\right) = 1.$$

For the numerical simulations, we have fixed initial conditions to be of the form

$$u^0(x) = \frac{\lambda_1 I_0}{\alpha_1} \exp\left(-\frac{\alpha_2 x^2}{2d\ell}\right), x \in [0,\ell],$$

with

$$(S_1^0, I_1^0, S_2^0, I_2^0) = \left(S_0 - I_0 - \int_0^\ell u^0(x)\mathrm{d}x, I_0, 1 - S_0, 0\right),$$

where S_0 and I_0 may vary. In Figures 6-7-8, S_0 and I_0 are fixed to $(S_0, I_0) = (1/2, 10^{-6})$, while in Figure 10, S_0 is allowed to vary and I_0 is fixed to $I_0 = 10^{-6}$.

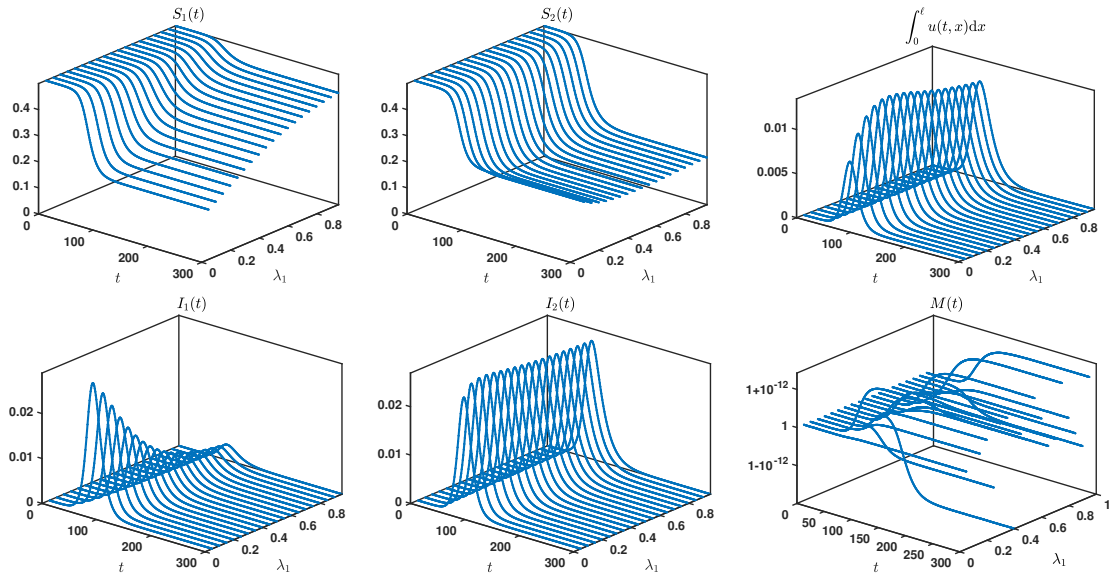

Figure 6: *Profiles of the solutions* $(S_i(t), I_i(t))$ *together with the total population on the edge* $\int_0^\ell u(t,x)\mathrm{d}x$ *and the total mass of the system* $M(t)$ *as the parameter* λ_1 *is varied from* 0.05 *to* 0.95*. All other parameters are fixed and set to* $d = \ell = 1$*,* $\lambda_2 = 1/10$*,* $\alpha_1 = \alpha_2 = 1/4$*, and* $\tau_1 = \tau_2 = 1$ *with* $\eta_1 = \eta_2 = 1/3$*. For the initial condition we have* $(S_0, I_0) = (1/2, 10^{-6})$*.*

In Figure 6, we report the profiles of the solutions $(S_i(t), I_i(t))$ together with the total population on the edge $\int_0^\ell u(t,x)\mathrm{d}x$ and the total mass of the system $M(t)$ as the parameter λ_1 is varied from 0.05 to 0.95, while all other parameters are being kept fixed. We observe that the dynamics of the epidemic at the second vertex is almost independent of the parameter λ_1 while it has a significant impact on the dynamics at the first vertex. Indeed, as λ_1 is increased, the maximum of infected individuals $\max_{t\geq 0} I_1(t)$ is decreased. In the last panel of the figure, we also illustrate the conservation of total population where the fluctuations around $M^0 = 1$ is of order 10^{-12}. In the top panel of Figure 7, we present the final total populations of infected individuals and corresponding final population of susceptible individuals as λ_1 is varied. The blue curve is the location of $(\mathcal{I}_1^\infty, \mathcal{I}_2^\infty)$ respectively (S_1^∞, S_2^∞) while the dark red circles indicate the numerically computed values. We recover the fact that λ_1 has a more significant impact on the final total populations at the first vertex than it has at the second vertex. The get a better understanding of the intricate dynamics between the epidemic at the two vertices, we also present the relative distance $\Delta\mathcal{T} := \mathcal{T}_2 - \mathcal{T}_1$ between time of maximal infection $\mathcal{T}_j$ in each population as λ_1 is varied. We observe that $\Delta\mathcal{T}$ is not monotone in λ_1, as it first decreases and then increases. But we also note that $\Delta\mathcal{T} < 0$ for $\lambda_1 \geq 0.1$ traducing the fact that the pick of the epidemic occurs at the second vertex before it does at the first vertex, although initially $I_2^0 = 0$. This illustrates the effect of the diffusion of infected individuals along the edge.

Similarly, in Figure 7, we report the final total populations of infected individuals and corresponding final population of susceptible individuals as λ_2 (second panel), α_1 (third panel) and α_2 (bottom panel) are varied from 0.05 to 0.95. As expected, the final total population of infected individuals

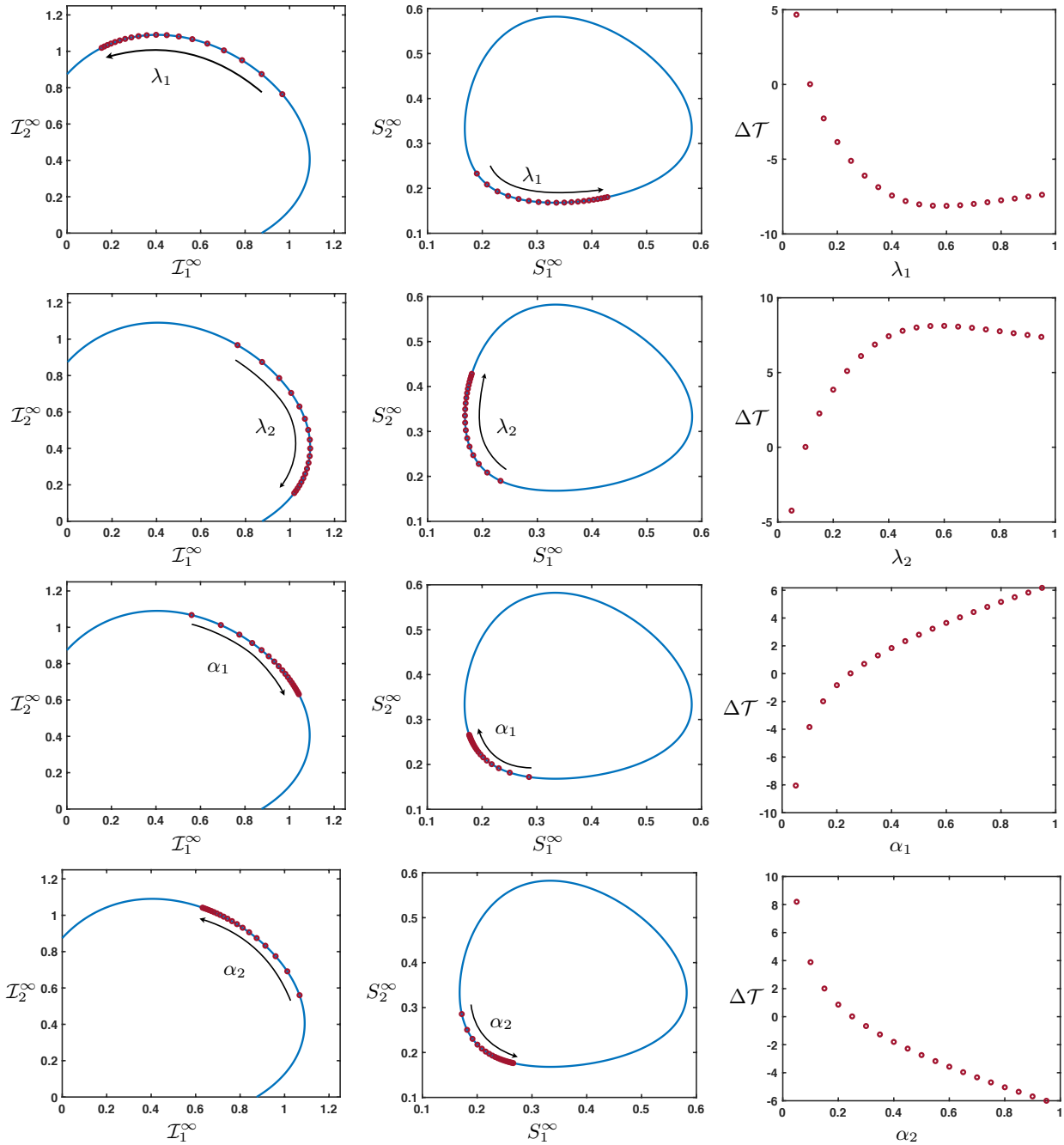

Figure 7: *Final total populations of infected individuals (left) and corresponding final population of susceptible individuals (middle) as one parameter is varied from* 0.05 *to* 0.95 *while all parameters are fixed. The blue curve is the location of* $(\mathcal{I}_1^\infty, \mathcal{I}_2^\infty)$ *respectively* (S_1^∞, S_2^∞) *while the dark red circles indicate the numerically computed values. Right: relative distance* $\Delta\mathcal{T} := \mathcal{T}_2 - \mathcal{T}_1$ *between time of maximal infection* $\mathcal{T}_j$ *in each population, indicated by dark red circles, as the parameter is varied from* 0.05 *to* 0.95*. Varying parameters:* λ_1 *(top panel),* λ_2 *(second panel),* α_1 *(third panel) and* α_2 *(bottom panel).*

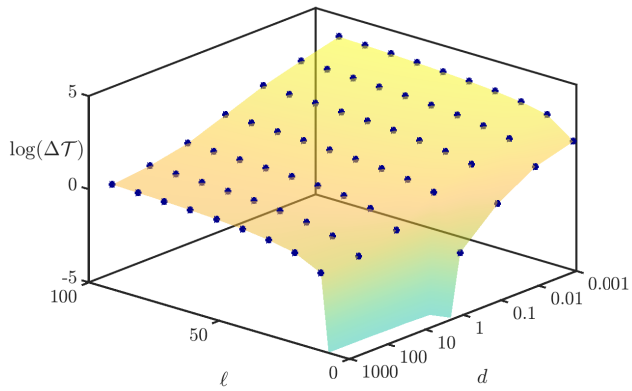

Figure 8: *Log-plot of the relative distance $\Delta\mathcal{T} = \mathcal{T}_2 - \mathcal{T}_1$ between time of maximal infection $\mathcal{T}_j$ in each population $I_j(t)$ as the diffusion coefficient d and the length of the edge ℓ are varied while all other parameters are fixed to $\lambda_1 = \lambda_2 = 1/10$, $\alpha_1 = \alpha_2 = 1/4$, and $\tau_1 = \tau_2 = 1$ with $\eta_1 = \eta_2 = 1/3$. For the initial condition we have $(S_0, I_0) = (1/2, 10^{-6})$. We note that as d becomes smaller $\Delta\mathcal{T}$ rapidly increases as ℓ increases.*

at the second vertex decreases as λ_2 increases while at the first vertex it varies less significantly. As α_1 increases, the final total population of infected individuals at the first vertex increases while it decreases at the second vertex. This time the relative distance $\Delta\mathcal{T} := \mathcal{T}_2 - \mathcal{T}_1$ between time of maximal infection is monotonically increasing with α_1. We get the opposite monotonicity properties as α_2 is varied.

In Figure 8, we investigate the joint effect of the diffusion coefficient d and the length of the edge ℓ on the dynamics of the epidemic at the vertices. Here, we focus on the delay between time of maximal infection $\mathcal{T}_j$ in each infected population $I_j(t)$. As expected, when the diffusion coefficient is really small while the length is being kept at order one, $\Delta\mathcal{T}$ takes large value: $\Delta\mathcal{T} \sim 10^4$ when $d = 10^{-3}$ and $\ell = 1$. Biologically, this means that when the diffusion coefficient is really small it takes more time for infected individuals from vertex one to reach the second vertex and start an epidemic. We also note that at fixed ℓ, $\Delta\mathcal{T}$ monotonically decreases as d increases, while at fixed d, $\Delta\mathcal{T}$ monotonically increases as ℓ increases.

In Figures 9-10, we vary respectively the initial population of susceptible individuals S_0 and infected individuals I_0. We visualize the final total populations of infected individuals and corresponding final population of susceptible individuals on the parameterized surfaces $(\mathcal{I}_1^\infty, \mathcal{I}_2^\infty, S_0)$ and $(S_1^\infty, S_2^\infty, S_0)$, respectively $(\mathcal{I}_1^\infty, \mathcal{I}_2^\infty, I_0)$ and $(S_1^\infty, S_2^\infty, I_0)$, where the level sets of the parameterized surface are given by the conservation of total mass (4.6). We note that $(\mathcal{I}_1^\infty, \mathcal{I}_2^\infty)$ and (S_1^∞, S_2^∞) are almost independent of I_0 when $I_0 \leq 10^{-3}$ with sensible variations only occurring for larger values of I_0. On the other hand, we observe that as S_0 is increased the final total population of infected individuals increases at the first vertex while it decreases at the second one. The dependence of (S_1^∞, S_2^∞) as a function of S_0 is more subtile and is presented in Figure 11. In the same figure, we also show the location of $\max I_j(t)$ and its amplitude. We observe a strong nonlinear dependence with respect to S_0. As S_0 increases, we first see that the time at which $I_1(t)$ is maximal increases and then decreases, while $\max I_1(t)$ is monotonically increasing. The converse is observed

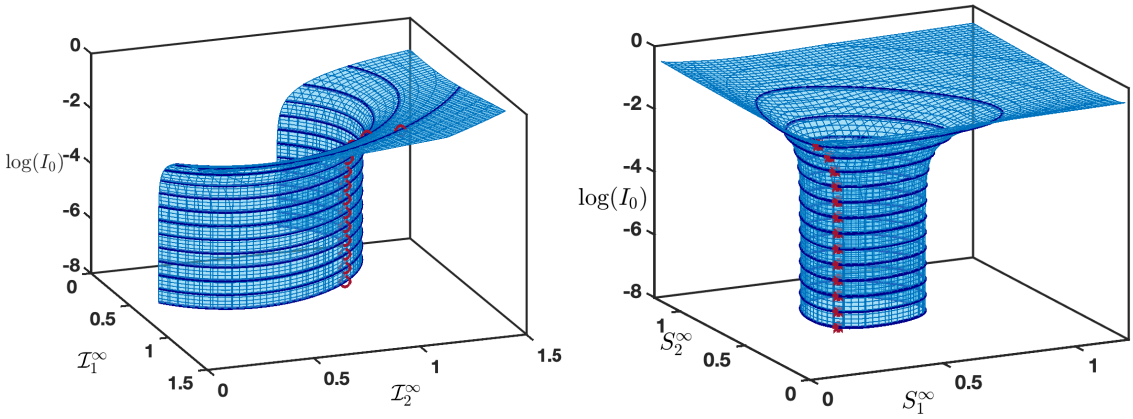

Figure 9: *Final total populations of infected individuals (left) and corresponding final population of susceptible individuals (right) as the initial population of susceptible individuals* I_0 *is varied from* 10^{-7} *to* 10^{-1} *in log-scale while* $S_0 = 1/2$ *is fixed. The dark blue curves are the location of* $(\mathcal{I}_1^\infty, \mathcal{I}_2^\infty)$ *respectively* (S_1^∞, S_2^∞) *for each value of* S_0*, while the dark red circles indicate the numerically computed values. Each dark blue curve is a level set of the parameterized surface given by the conservation of total mass* (4.6)*. All other parameters are fixed to* $d = \ell = 1$*,* $\lambda_1 = \lambda_2 = 1/10$*,* $\alpha_1 = \alpha_2 = 1/4$*, and* $\tau_1 = \tau_2 = 1$ *with* $\eta_1 = \eta_2 = 1/3$*.*

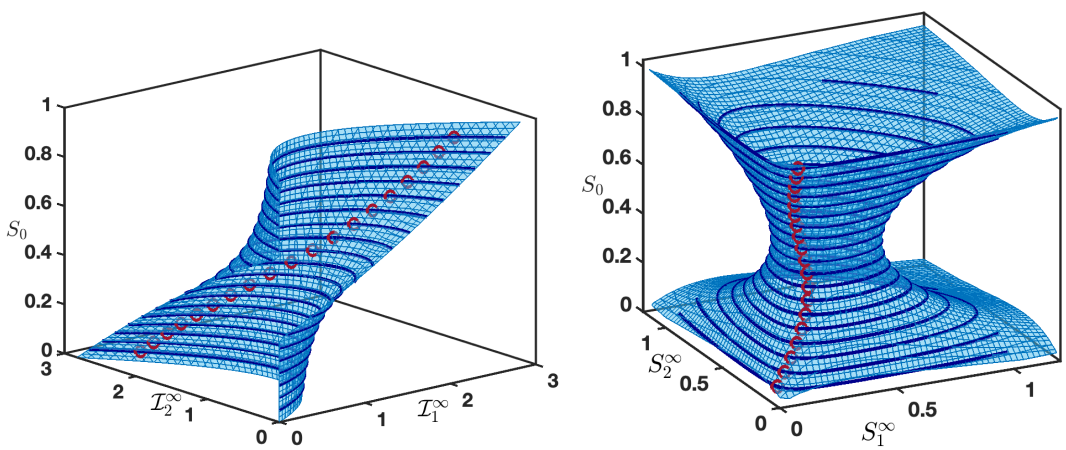

Figure 10: *Final total populations of infected individuals (left) and corresponding final population of susceptible individuals (right) as the initial population of susceptible individuals* S_0 *is varied from* 0.05 *to* 0.95 *while* $I_0 = 10^{-6}$ *is fixed. The dark blue curves are the location of* $(\mathcal{I}_1^\infty, \mathcal{I}_2^\infty)$ *respectively* (S_1^∞, S_2^∞) *for each value of* S_0*, while the dark red circles indicate the numerically computed values. Each dark blue curve is a level set of the parameterized surface given by the conservation of total mass* (4.6)*. All other parameters are fixed to* $d = \ell = 1$*,* $\lambda_1 = \lambda_2 = 1/10$*,* $\alpha_1 = \alpha_2 = 1/4$*, and* $\tau_1 = \tau_2 = 1$ *with* $\eta_1 = \eta_2 = 1/3$*.*

at the second vertex.

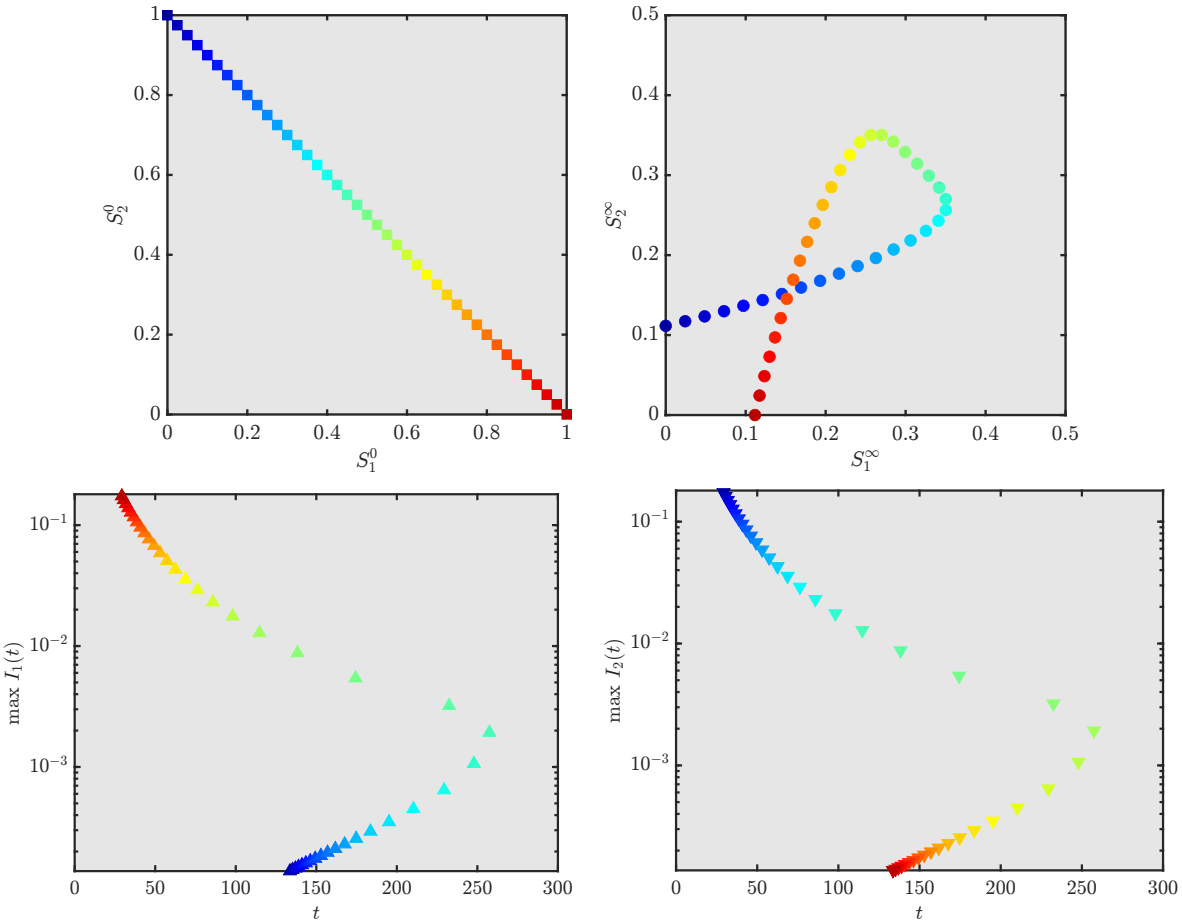

Figure 11: *Locations of* $S_{1,2}^\infty$ *(top) and* $\max I_{1,2}(t)$ *(bottom left and right) as functions of* $S_{1,2}^0$*. Values of all other parameters are similar to Figure 10. The initial condition is of the form* $(S_0, 1 - S_0)$ *with* $S_0 \in [0, 1]$ *and to each initial configuration is associated a color code from blue to red. The curve in the top right panel is a projection on the* (S_1^∞, S_2^∞)*-plane of the parametrized a curve from Figure 10, right panel.*

6.2 Case of 3 vertices and 3 edges

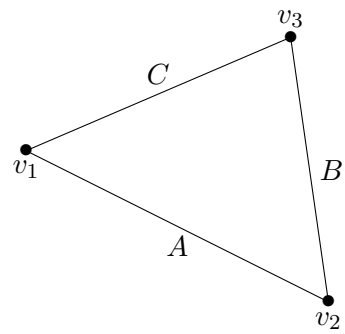

Next, we consider the case of 3 vertices and 3 edges arranged in a triangular configuration. For the numerical simulations presented in Figure 12, we have assumed full symmetry in the parameters that is

$$(\ell_e, d_e) = (\ell, d), \quad e \in \mathcal{E}, \quad (\tau_v, \eta_v) = (\tau, \eta), \quad v \in \mathcal{V},$$
$$(\alpha_e^v, \lambda_e^v) = (\alpha, \lambda), \quad (e, v) \in \mathcal{E} \times \mathcal{V}, \quad \nu_{e,e'}^v = \nu, \quad (e, e', v) \in \mathcal{E} \times \mathcal{E} \times \mathcal{V}.$$

Regarding the initial condition, we have chosen

$$(S_1^0, I_1^0, S_2^0, I_2^0, S_3^0, I_3^0) = \big(S^0 - I_0, I_0, S^0, 0, S^0, 0\big) \quad v \in \mathcal{V},$$

for a given (S^0, I_0), while for each $e \in \mathcal{E}$ we have set $u_e^0(x) = 0$ on Ω_e. Note that, we have initially a boundary layer as our initial condition does not satisfy (2.3) for small times. We remark that the final total populations of infected individuals and corresponding final population of susceptible individuals belong to a surface as provided by (4.6)-(4.7) from Theorem 2.

In Figure 13, we tested a different configuration. Upon labeling by A the edge between vertices v_1 and v_2, B the edge between vertices v_2 and v_3 and C the edge between vertices v_1 and v_3, we have set the parameters to

$$\alpha_A^1 = \alpha_B^2 = \alpha_C^3 = 0, \text{ and } \alpha_A^2 = \alpha_B^3 = \alpha_C^2 = 1/10,$$

while

$$\lambda_A^1 = \lambda_B^2 = \lambda_C^3 = 1/20, \text{ and } \lambda_A^2 = \lambda_B^3 = \lambda_C^2 = 0,$$

and

$$\nu_{A,C}^1 = \nu_{B,A}^2 = \nu_{C,B}^3 = 0, \text{ and } \nu_{C,A}^1 = \nu_{A,B}^2 = \nu_{B,C}^3 = 1/30.$$

The length of each edge is fixed $\ell_e = \ell = 1$ and $(\tau_v, \eta_v) = (1, 1/7)$ at each vertex $v \in \mathcal{V}$. Finally, we have set different coefficients on each edge, namely $d_A = 1$, $d_B = 10^{-2}$ and $d_C = 10^{-3}$. Initially, we assume that infected individuals are only present at vertex v_1 and each vertex has the same number of susceptible individuals fixed to $1/3$. Finally, for each $e \in \mathcal{E}$ we have set $u_e^0(x) = 0$ on Ω_e. We see in Figure 13 that such a configuration can generate a second wave of infection at the first and second vertices showing that transient dynamics can be complex with multiple bumps of infection.

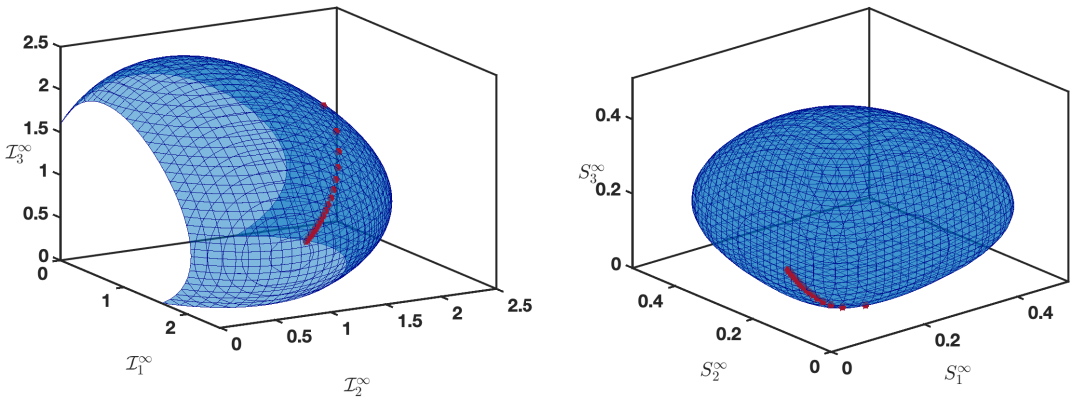

Figure 12: *Final total populations of infected individuals (left) and corresponding final population of susceptible individuals (right) as* ν *is varied from* 0.05 *to* 0.95*. The dark blue surfaces are the location of* $(\mathcal{I}_1^\infty, \mathcal{I}_2^\infty, \mathcal{I}_3^\infty)$ *respectively* $(S_1^\infty, S_2^\infty, S_3^\infty)$ *for each value of* S_0*, while the dark red circles indicate the numerically computed values. Parameters were set to* $\ell = d = 1$*,* $(\tau, \eta) = (1, 1/6)$*, and* $(\alpha, \lambda) = (1/8, 1/10)$*, while the initial condition is* $(S_0, I_0) = (1, 10^{-6})$*.*

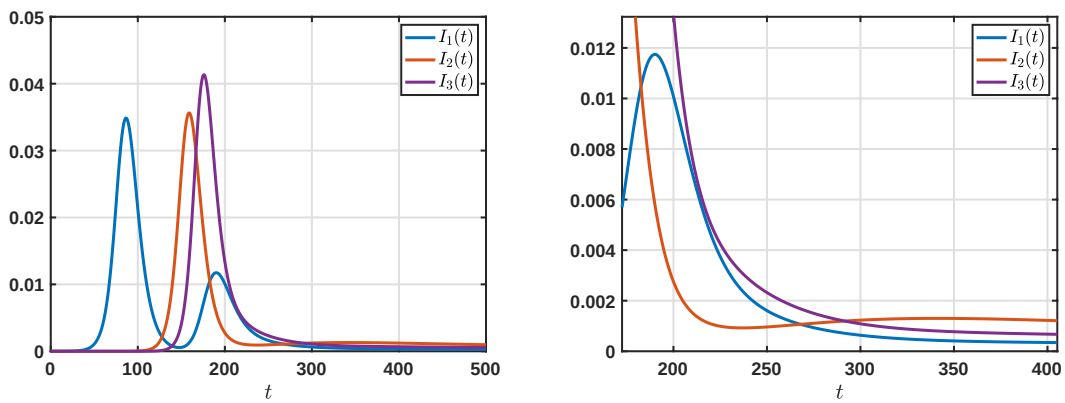

Figure 13: *Time plot of infected populations in the case of* 3 *vertices and* 3 *edges in a triangular configuration between times* $[0, 500]$ *(left) and a zoom for times between* $[150, 400]$ *(right). We observe a second wave of infection at the first vertex resulting from incoming infected individuals that have successively passed through the two other vertices. This second wave is also present at the second vertex with a slight increase of* $I_2(t)$ *after the second wave has reached the first vertex. Parameters values are set in the text.*

6.3 Case of 4 vertices and 3 edges

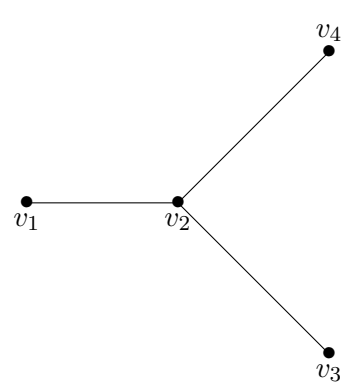

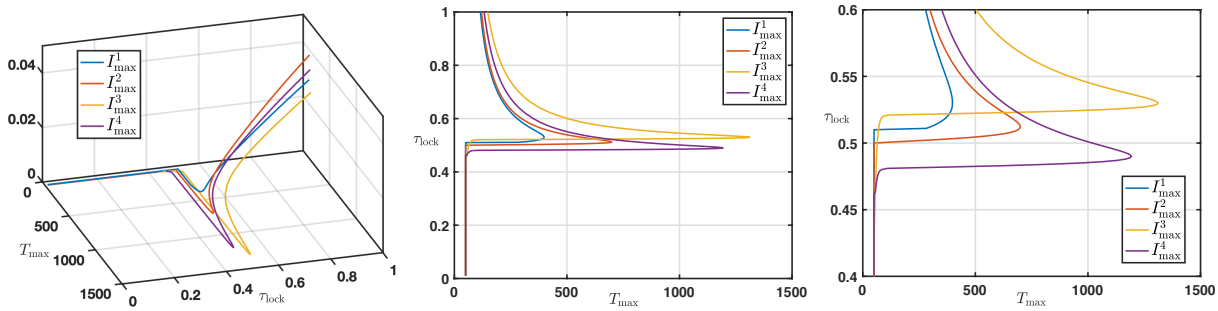

Figure 14: *Location of the time of maximal infection T_{max} for each vertex together with the corresponding amplitude I^j_{max} as a function of τ_{lock} (left) with its projection in the (T_{max}, τ_{lock})-plane (middle) and a zoom near the turning points (right). Other parameters are set to $\ell = 1$, $d = 0.1$, $\eta = 1/8$, $(\alpha, \lambda, \nu) = (1/8, 1/20, 1/20)$, $T_{lock} = 50$ and $\mu_{lock} = 100$ with $(S_0, I_0, \epsilon) = (1/4, 10^{-6}, 10^{-2})$.*

Next, we consider a star-shape graph with 4 vertices and 3 edges where one vertex is connected to the three others. In this configuration, we assume that our parameters may vary with respect to time, modeling locked down strategies for example [11, 16]. More precisely, we will assume that there exists T_{lock} and μ_{lock} such that the transmission rates can be written as

$$\tau_v(t) = \begin{cases} \tau\,, & t \in [0, T_{lock}], \\ \frac{\tau \exp(-\mu_{lock}(t - T_{lock})) + \tau_{lock}}{1 + \exp(-\mu_{lock}(t - T_{lock}))}\,, & t > T_{lock}, \end{cases}$$

for each $v \in \mathcal{V}$ and for a given $0 < \tau_{lock} < \tau$. We will assume that the four vertices are at equal distance such that $\ell_e = \ell$ for each $e \in \mathcal{E}$ and that the coefficient diffusion are equal on each edge, $d_e = d$, $e \in \mathcal{E}$. We further assume that at the central vertex v_2 exchanges are no longer allowed. That is, we impose that

$$\alpha^2_e = \begin{cases} \alpha\,, & t \in [0, T_{lock}], \\ \alpha \exp(-\mu_{lock}(t - T_{lock}))\,, & t > T_{lock}, \end{cases} \qquad e \in \mathcal{E},$$

while $\alpha^j_e = \alpha$ for $j \neq 2$ and $e \in \mathcal{E}$, together with

$$\lambda^2_e = \begin{cases} \lambda\,, & t \in [0, T_{lock}], \\ \lambda \exp(-\mu_{lock}(t - T_{lock}))\,, & t > T_{lock}, \end{cases} \qquad e \in \mathcal{E},$$

while $\lambda^j_e = \lambda$ for $j \neq 2$ and $e \in \mathcal{E}$, and also

$$\nu^2_{e,e'} = \begin{cases} \nu\,, & t \in [0, T_{lock}], \\ \nu \exp(-\mu_{lock}(t - T_{lock}))\,, & t > T_{lock}, \end{cases} \qquad (e, e') \in \mathcal{E} \times \mathcal{E}.$$

Finally, we set $\eta_v = \eta$ for all $v \in \mathcal{V}$. Regarding the initial condition, we work with

$$(S^0_1, I^0_1, S^0_2, I^0_2, S^0_3, I^0_3, S^0_4, I^0_4) = (S_0 - I_0, I_0, S_0, 0, S_0 - \epsilon, 0, S_0 + \epsilon, 0)\,,$$

for given (S_0, I_0, ϵ), while for each $e \in \mathcal{E}$ we have set $u^0_e(x) = 0$ on Ω_e.

In Figure 14, we report the location of the time of maximal infection T_{max} for each vertex together with the corresponding amplitude $I^j_{max} = \max_{t \geq 0} I_j(t)$ as a function of τ_{lock}. We observe that

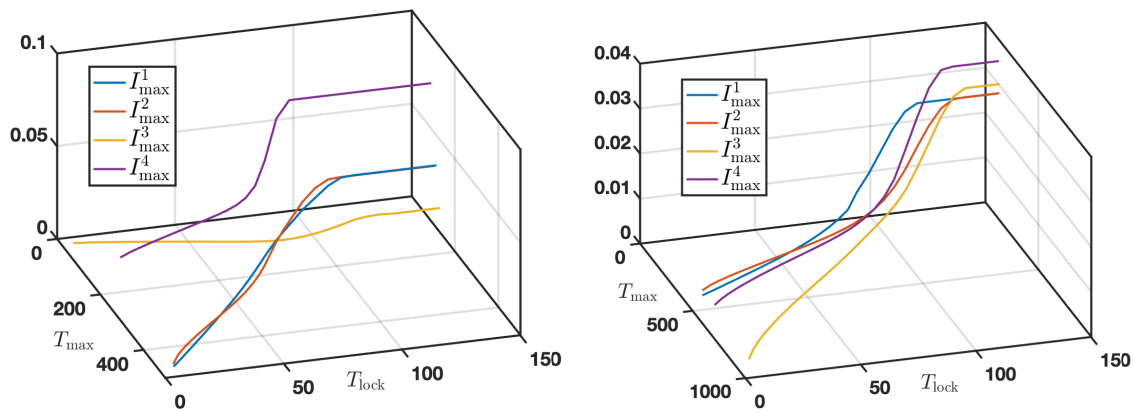

Figure 15: *Location of the time of maximal infection T_{max} for each vertex together with the corresponding amplitude I^j_{max} as a function of T_{lock} for two configurations of initial susceptible populations at vertices v_3 and v_4, with $\epsilon = 10^{-1}$ (left) and $\epsilon = 10^{-2}$ (right). Other parameters are set to $\ell = 1$, $d = 0.1$, $\eta = 1/8$, $(\alpha, \lambda, \nu) = (1/8, 1/20, 1/20)$, $T_{lock} = 50$ and $\eta_{lock} = 0.6$ with $(S_0, I_0) = (1/4, 10^{-6})$.*

below a critical value of τ_{lock}, the time of maximal infection always occurs at $t = T_{max} = T_{lock}$ traducing the fact that the locked down strategy has no effect on the dynamics of the epidemic. At each vertex, we observe the same pattern: as τ_{lock} is decreased the corresponding I^j_{max} is decreasing while T_{max} is increasing up to some value of τ_{lock} where we observe a sudden turning point (see the right panel of Figure 14). We observe that τ^{tp}_{lock,v_k}, the value of the turning point, is well approximated (actually always bounded by below) by the value at which the effective reproduction number of each vertex is equal to 1. Indeed we have $\mathscr{R}_{e,v_k} = 1$ if and only if $\tau^c_{v_k} = \frac{\eta_{v_k}}{S^0_{v_k}}$, and we find

$$\tau^c_{v_1} \simeq 0.5, \quad \tau^c_{v_2} = 0.5, \quad \tau^c_{v_3} \simeq 0.52, \quad \text{and} \quad \tau^c_{v_4} \simeq 0.48,$$

with our specific values of the initial condition, while we have computed

$$\tau^{tp}_{lock,v_1} \simeq 0.53, \quad \tau^{tp}_{lock,v_2} \simeq 0.51, \quad \tau^{tp}_{lock,v_3} \simeq 0.53, \quad \text{and} \quad \tau^{tp}_{lock,v_4} \simeq 0.49.$$

We also point out that when τ_{lock} is below the turning point τ^{tp}_{lock,v_k}, the corresponding value of I^j_{max} is below 10^{-3}. On the other hand, in Figure 15, we present similar results but this time τ_{lock} is fixed and T_{lock} varies. Above some critical value of T_{lock}, I^j_{max} saturates to a fixed value independent of T_{lock} traducing the fact that the locked down strategy has no effect on the dynamics of the epidemic if it occurs to late in time. Depending on the initial configuration of susceptible populations at each vertex, we observe intricate nonlinear relationships on the location of the time of maximal infection T_{max}.

6.4 Case of $N+1$ vertices and N edges

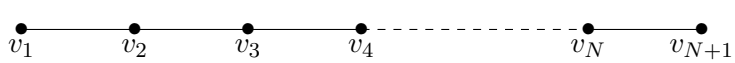

In our final example, we have considered a network of $N+1$ vertices and N edges arranged in a lattice, in the sense that vertex v_j is only connected to vertices v_{j-1} and v_{j+1} via two different edges.

Figure 16 shows the time evolution of the infected population $I_{v_j}(t)$ and susceptible populations $S_{v_j}(t)$ at each vertex for several different initial conditions when the length and diffusion coefficient of each edge are equal. In the first case (top panel), we assume that $I^0_{v_1} > 0$ while $I^0_{v_j} = 0$ for all other vertices, and observe a propagation of burst of activity among infected and susceptible populations. In the second case (middle panel), we assume that $I^0_{v_{\lfloor N/2 \rfloor}} > 0$ while $I^0_{v_j} = 0$ for all other vertices, and we see the propagation of two bursts of activity among infected and susceptible populations going leftwards and rightwards. In the last case (bottom panel), we assume that $I^0_{v_1} = I^0_{v_{N+1}} > 0$ while $I^0_{v_j} = 0$ for all other vertices, and we note the propagation of two waves activity which collide at the middle vertex $v_{\lfloor N/2 \rfloor}$. For very small values of the diffusion coefficient d, this burst of epidemic activity seems to travel coherently and forms a coherent traveling wave, as can be seen in Figure 17 where we represent the location of $\max_{t>0} I_{v_j}(t)$ at each vertex. Such a traveling wave of epidemic activity share similarities with traveling waves in excitable media such as the propagation of electrical activity along a nerve cell [13, 14] or calcium waves [24]. When $d = 10^{-3}$, they are all aligned on the same line, where for smaller values $d \in \left\{10^{-1}, 10^{-2}\right\}$ the location is a nonlinear curve. We also demonstrate that larger diffusion coefficient leads to a faster propagation of epidemic burst across vertices. Finally, we also remark that if $I^d_{\max,1}$ denotes the maximum as a function of d at the first vertex, we have $I^{d_1}_{\max,1} \leq I^{d_2}_{\max,1}$ for $d_1 \leq d_2$ while for larger vertices $j \geq 6$ we have the reverse ordering $I^{d_1}_{\max,j} \geq I^{d_2}_{\max,j}$ for $d_1 \leq d_2$.

For the numerical simulations presented in Figures 16-17, we have assumed full symmetry in the parameters that is

$$
\begin{aligned}
&(\ell_e, d_e) = (\ell, d), \quad e \in \mathcal{E}, \quad (\tau_v, \eta_v) = (\tau, \eta), \quad v \in \mathcal{V}, \\
&(\alpha^v_e, \lambda^v_e) = (\alpha, \lambda), \quad (e, v) \in \mathcal{E} \times \mathcal{V}, \quad \nu^v_{e,e'} = \nu, \quad (e, e', v) \in \mathcal{E} \times \mathcal{E} \times \mathcal{V}.
\end{aligned}
$$

Regarding the initial condition on the edge, we have set $u^0_e(x) = 0$ on Ω_e for each $e \in \mathcal{E}$.

Acknowledgment

This works was partially supported by Labex CIMI under grant agreement ANR-11-LABX-0040.

References

[1] D. G. Aronson. The asymptotic speed of propagation of a simple epidemic. *Res. Notes Math.*, 14, pp. 1-23, 1977.

[2] F. Ball and T. Britton. Epidemics on networks with preventive rewiring. ArXiv , arXiv:2008.06375, 2020.

[3] H. Berestycki, J.-M. Roquejoffre and L. Rossi. Propagation of epidemics along lines with fast diffusion. *Bull. Math. Biol.* to appear, 2020.

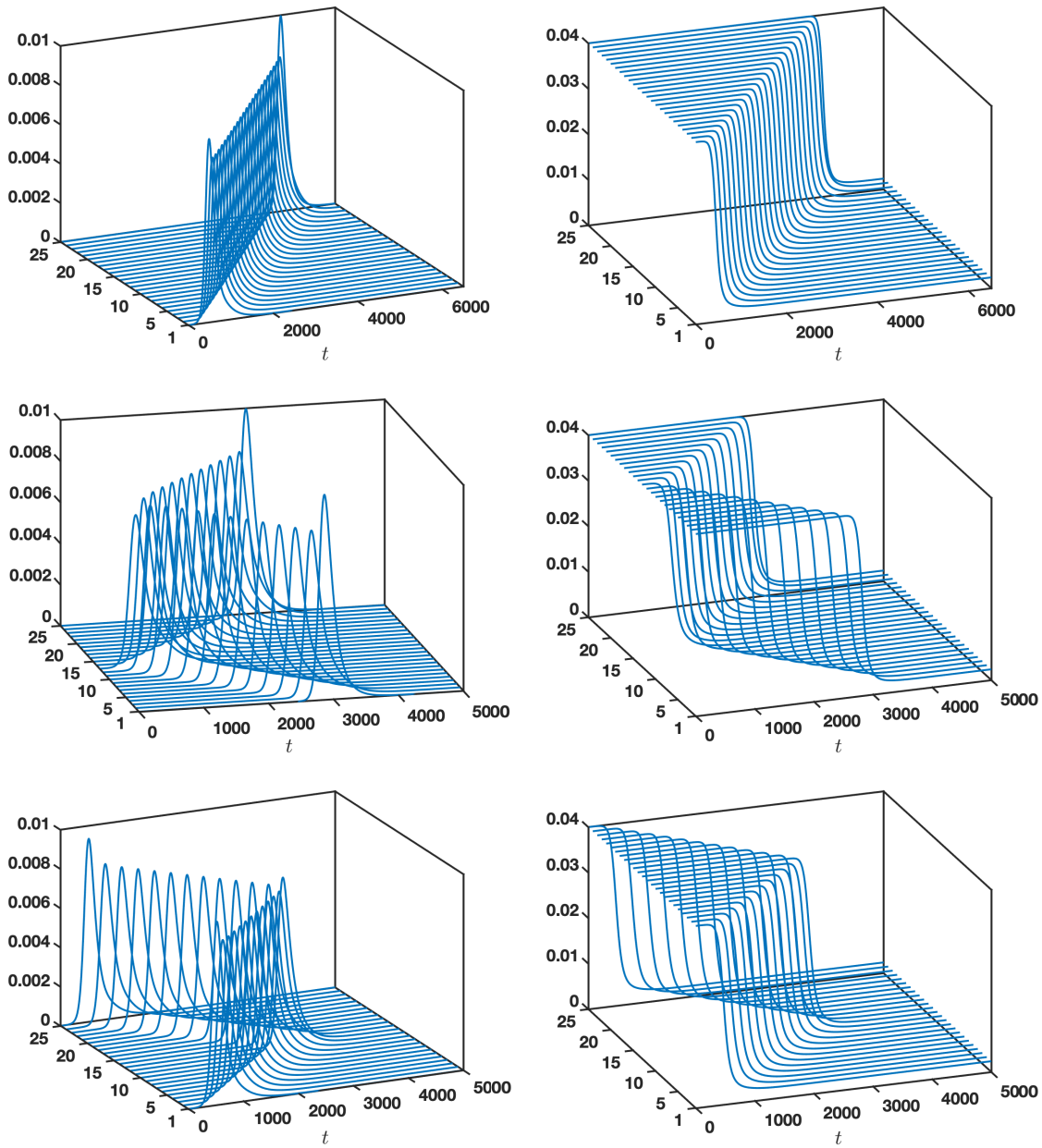

Figure 16: *Time evolution of the infected (left) population $I_j(t)$ and susceptible (right) populations $S_j(t)$ at each vertex for several different initial conditions and $N = 24$. Top: infected individuals are initially present only at vertex. Middle: infected individuals are initially present only at the middle vertex. Bottom: infected individuals are initially present only at the first and last vertices. We observe a traveling wave of infectious activity propagating though the vertices. Parameters were set to $\ell = 1$, $d = 10^{-3}$, $(\tau, \eta) = (1, 1/75)$, and $(\alpha, \lambda, \nu) = (1/8, 1/10, 1/20)$, while the initial condition is $(S_0, I_0) = (1/25, 10^{-6})$.*

[4] L. Bonnasse-Gahot, H. Berestycki, M.-A. Depuiset, M. B. Gordon, S. Roché, N. Rodriguez, and J.-P. Nadal. Epidemiological modelling of the 2005 French riots: a spreading wave and the role of contagion. *Scientific Reports*, 8, 2018.

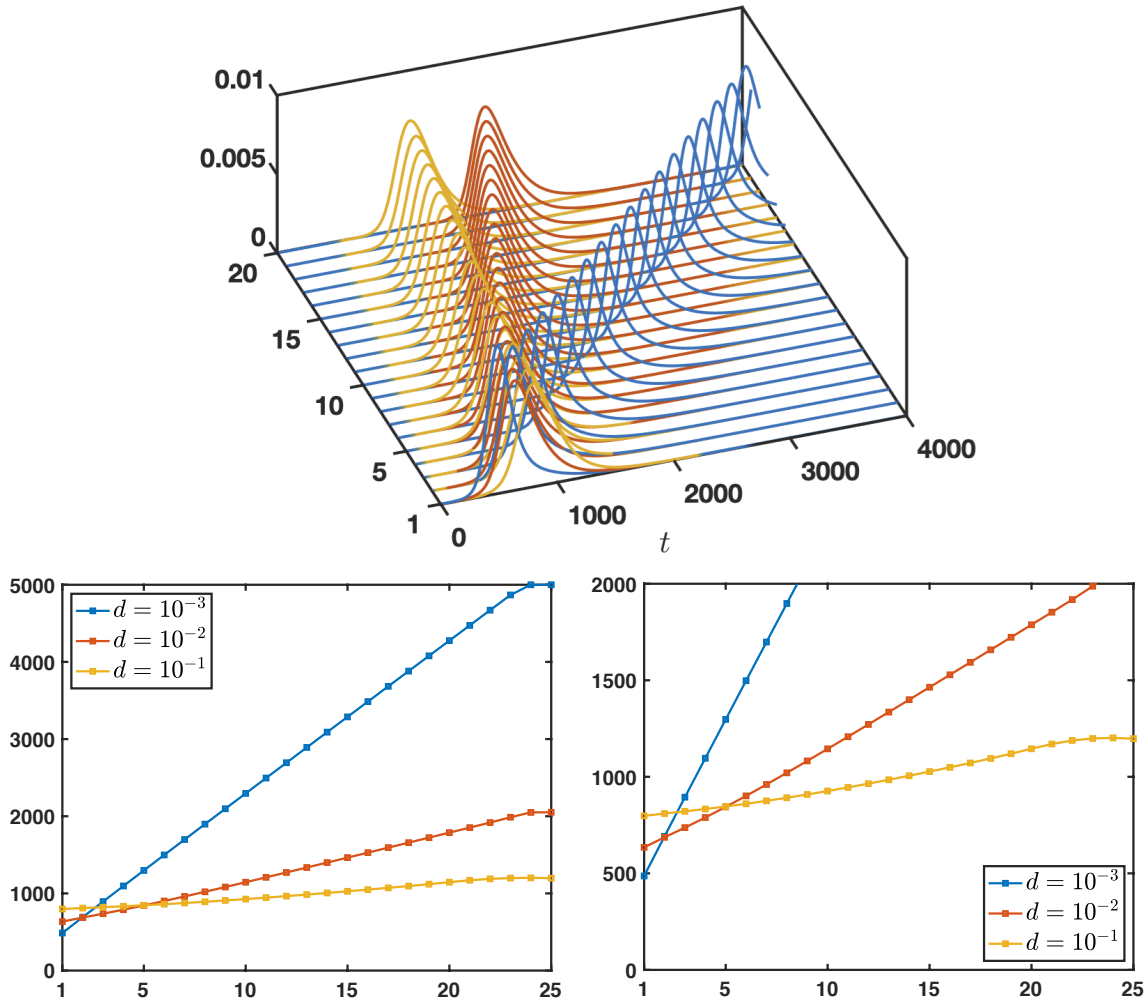

Figure 17: *Left: Location of the maxima of the infected population $I_j(t)$ at each vertex $j \in \{1, \cdots, 25\}$ for several different diffusion coefficients $d \in \{10^{-3}, 10^{-2}, 10^{-1}\}$. Right: Zoom of the left figure for small times. We observe that for very small d the location of the maxima is a long a line while it is curved for larger values of d. We also remark that if $I^d_{\max,1}$ denotes the maximum as a function of d at the first vertex, we have $I^{d_1}_{\max,1} \leq I^{d_2}_{\max,1}$ for $d_1 \leq d_2$ while for larger vertices $j \geq 6$ we have the reverse ordering $I^{d_1}_{\max,j} \geq I^{d_2}_{\max,j}$ for $d_1 \leq d_2$. Other parameters were set to $\ell = 1$, $(\tau, \eta) = (1, 1/75)$, and $(\alpha, \lambda, \nu) = (1/8, 1/10, 1/20)$, while the initial condition is $(S_0, I_0) = (1/25, 10^{-6})$.*

[5] T. Britton, M. Deijfen, M. Lindholm, and A. Nordvall Lageras. Epidemics on random graphs with tunable clustering. *J. Appl. Prob.*, 45, 743-756, 2008.

[6] Centers for Disease Control and Prevention . Severe acute respiratory syndrome – Singapore, 2003. *Morbidity and mortality weekly report* 52.18, 405, 2003.

[7] R.M. Corless, G.H. Gonnet, D.E. Hare, D.J. Jeffrey and D.E. Knuth. On the LambertW function. *Advances in Computational mathematics,* 5(1), 329-359, 1996.

[8] JF David, SA Iyaniwura, MJ Ward and F Brauer. A novel approach to modelling the spatial

spread of airborne diseases: an epidemic model with indirect transmission. *Mathematical Biosciences and Engineering,* 17(4):3294, 2020.

[9] O. Diekmann. Thresholds and travelling waves for the geographical spread of infection. *J. Math. Biol.*, 6, pp. 109-130, 1978.

[10] O. Diekmann, J.A.P. Heesterbeek, J.A.J. Metz. On the definition and the computation of the basic reproduction ratio $R0$ in models for infectious diseases in heterogeneous populations. *J. Math. Biol.*, 28, p. 365, 1990.

[11] Q. Griette, P. Magal and O. Seydi. Unreported cases for Age Dependent COVID-19 Outbreak in Japan. *Biology* 9, 132, 2020.

[12] H.W. Hethcote. The mathematics of infectious diseases. *SIAM Rev.* 42 (4) 599–653, 2000.

[13] A.L. Hodgkin and A.F. Huxley. A quantitative description of membrane current and its application to conduction and excitation in nerve. *Journal of Physiology,*117, pages 500–544, 1952.

[14] H.J. Hupkes and B. Sandstede. Traveling pulse solutions for the discrete FitzHugh-Nagumo system. *SIAM J. Applied Dynamical Systems,* vol 9, no 3, pages 827–882, 2010.

[15] W. O. Kermack, A. G. McKendrick. A contribution to the mathematical theory of epidemics. *Proc. Roy. Sot. Ser. A*, 115, pp. 700-721, 1927.

[16] Z. Liu, P. Magal, O. Seydi, and G. Webb. Predicting the cumulative number of cases for the COVID-19 epidemic in China from early data. *Mathematical Biosciences and Engineering*, 17(4), 3040-3051, 2020.

[17] P. Magal, O. Seydi and G. Webb. Final size of a multi-group SIR epidemic model: Irreducible and non-irreducible modes of transmission. *Mathematical Biosciences* 301, 59-67, 2018.

[18] P. Magal, O. Seydi and G. Webb. Final size of an epidemic for a two group SIR model. *SIAM Journal on Applied Mathematics*, 76, 2042-2059, 2016.

[19] S. Mandal, R.R. Sarkar and S. Sinha. Mathematical models of malaria - a review. *Malaria Journal,* 10:202, 1-19, 2011.

[20] P. Magal and G. Webb. The parameter identification problem for SIR epidemic models: Identifying Unreported Cases. *Journal of Mathematical Biology,* 77(6-7), 1629–1648, 2018.

[21] New England Journal of Medicine. *Letter to the Editor,* DOI: 10.1056/NEJMc2001468, January 30, 2020.

[22] T. Reluga. A two-phase epidemic driven by diffusion. *Journal of theoretical biology,* 229.2: 249-261, 2004.

[23] M. Sekiguchi and I. Emiko. Dynamics of a discretized SIR epidemic model with pulse vaccination and time delay. *Journal of Computational and Applied Mathematics*, 236.6: 997-1008, 2011.

[24] J. Sneyd. Tutorials in Mathematical Biosciences II. *Lecture Notes in Mathematics, chapter Mathematical Modeling of Calcium Dynamics and Signal Transduction,* Volume 187, Berlin Heidelberg, New York: Springer, 2005.

[25] K. Spricer and T. Britton. An epidemic model on a weighted network. *Network Science,* 7:556-580, 2019.

[26] P. Van den Driessche and J. Watmough. Reproduction numbers and sub-threshold endemic equilibria for compartmental models of disease transmission. *Mathematical biosciences,* 180.1-2: 29-48, 2002.